Ligand-Induced Changes in Estrogen Receptor Conformation As Measured by Site-Directed Spin Labeling†

Kyle M. Hurth, Mark J. Nilges, Kathryn E. Carlson, Anobel Tamrazi, R. Linn Belford, and John A. Katzenellenbogen*

Department of Chemistry, University of Illinois, 600 South Mathews Avenue, Urbana, Illinois 61801

Received September 2, 2003; Revised Manuscript Received November 19, 2003

ABSTRACT: Site-directed spin labeling (SDSL), the site-specific incorporation of nitroxide spin-labels into a protein, has allowed us to investigate ligand-induced conformational changes in the ligand-binding domain of human estrogen receptor α (hERα-LBD). EPR (electron paramagnetic resonance) spectroscopy of the nitroxide probe attached to ER produces different spectra depending upon the identity of the bound ligand; these differences are indicative of changes in the type and degree of motional character of the spin-label induced by different ligand-induced conformations of labeled ER. Visual inspection of EPR spectra, construction of *B* versus *C* cross-correlation plots, and cross-comparison of spectral pairs using a relative squared difference (RSD) calculation allowed receptor−ligand complexes to be profiled according to their conformational character. Plotting *B* and *C* parameters allowed us to evaluate the liganded receptor according to the motional characteristics of the attached spin-label, and they were particularly illustrative for the receptor labeled at position 530, which had motion between the fast and intermediate regimes. RSD analysis allowed us to directly compare the similarity or difference between two different spectra, and these comparisons produced groupings that paralleled those seen in *B* versus *C* cross-correlation plots, again relating meaningfully with the pharmacological nature of the bound ligand. RSD analysis was also particularly useful for qualifying differences seen with the receptor labeled at position 417, which had motion between the intermediate and slow motional regimes. This work demonstrates that *B* and *C* formulas from EPR line shape theory are useful for qualitative analysis of spectra with differences subtler than those that are often analyzed by EPR spectroscopists. This work also provides evidence that the ER can exist in a range of conformations, with specific conformations resulting from preferential stabilization of ER by the bound ligand. Furthermore, it documents the complexity and uniqueness of the ligand−receptor structure, and highlights the fact that structural differences exist between the receptor bound with ligands of different pharmacological character that, nevertheless, produce similar crystal structures.

Estrogens play numerous roles in growth, development, and disease. Their action is thought to proceed through the estrogen receptor (ER),[1] a ligand-regulated transcription factor, of which there are two known mammalian ER subtypes, ERα and ER*β*. ER has a domain organization that is characteristic of the nuclear hormone receptor gene superfamily: an N-terminal activation function, a centrally located DNA binding domain, a hinge region, and a C-terminal ligand-binding domain that is responsible for receptor dimerization and contains a ligand-dependent activation function (*1*, *2*).

Although there is emerging evidence that the ER can function through nongenomic pathways (*3*), its principal action is still thought to be through genomic mechanisms. In both of these processes, the ligand plays a critical role, since ligand binding to ER leads to changes in receptor conformation that trigger the recruitment of coregulator proteins and subsequent modulation of gene transcription (*4*). Thus, determining the relationship between ligand structure and the conformational changes induced in ER is funda-

† We are grateful for support of this work through grants from the National Institutes of Health (PHS 5R37 DK15556 to J.A.K. and P41-RR01811 and R01-RR01811 to R.L.B.).

* To whom correspondence should be addressed: Department of Chemistry, University of Illinois, 600 S. Mathews Ave., Urbana, IL 61801. Phone: (217) 333-6310. Fax: (217) 333-7325. E-mail: jkatzene@uiuc.edu.

[1] Abbreviations: CME_2, chloromethyl estradiol; cyc, cyclofenil; DMF, *N*,*N*-dimethylformamide; E_1, estrone; E_2, estradiol; E_3, estriol; EPR, electron paramagnetic resonance; ER, estrogen receptor; ESI FT-ICR MS, electrospray ionization Fourier transform-ion cyclotron resonance mass spectrometry; GRIP-1, glucocorticoid receptor interacting protein-1; HAP, hydroxyapatite; hERα-LBD, human estrogen receptor α ligand-binding domain; IT, 4-(2-iodoacetamido)TEMPO; *IT-C417*, estrogen receptor labeled with iodoacetamidoTEMPO at position 417; *IT-C530*, estrogen receptor labeled with iodoacetamidoTEMPO at position 530; C381S/C417S/C530S, triple mutant which is unreactive to labeling, which has been subjected to the same labeling procedure as *IT-C530* and *IT-C417*; MALDI-TOF MS, matrix-assisted laser desorption ionization time-of-flight mass spectrometry; MP, 3-maleimidoPROXYL; MTSL, methanethiosulfonate spin-label; P1496, α-zearalanol; pyr-ag, ethyl-pyrazole-triol agonist; pyr-antag, ethyl-pyrazole-triol antagonist; ral, raloxifene; RSD, relative squared difference; SC, shortened chain label; SDSL, site-directed spin labeling; SERMs, selective estrogen receptor modulators; SRC-1, steroid receptor coactivator-1; T/G buffer, Tris-glycerol buffer; TOT, 4-*trans*-hydroxytamoxifen.

10.1021/bi035566p CCC: $27.50
Published on Web 01/29/2004

mental to understanding both the mechanistic details of estrogen action and the intriguing tissue-selective pharmacology of these hormones.

The conformation of nuclear hormone receptor ligand complexes has been investigated with protease sensitivity assays (*5*−*14*), interactions with coregulators (*15*−*20*), phage-displayed peptides (*21*−*23*), and NMR spectroscopy (*24*, *25*). However, the most detailed picture of receptor conformation has come from X-ray crystallography (*26*−*29*), and currently, 10 crystal structures of the ligand-binding domain of ERα and ER*β* (involving six different ligands) have been published (*30*). From these structures, the ligand-dependent orientation of a C-terminal helix (helix 12) has emerged as the principal determinant that distinguishes the function of estrogens from antiestrogens. In the ER complexes with estrogens, the position of helix 12 creates a coactivator binding site, whereas the position of helix 12 in ER−antiestrogen complexes blocks coactivator binding (*28*). Unfortunately, no crystal structure of the unliganded receptor (apo) exists, and there is a lack of structures for ER bound with other interesting ligands.

It is now becoming clear that the complex pharmacology of estrogens cannot be fully explained by the two alternative, static conformations of the ER ligand-binding domain shown by X-ray crystallography. More dynamic models for ligand regulation of the ER conformation have been proposed (*31*). Thus, additional methods are needed for evaluating not only ligand-induced conformational changes in ER but also how ligand binding affects ER conformational dynamics. Methods that can be used to evaluate receptor dynamics should improve our understanding of the molecular mechanism by which ligands function through the ER.

One known method of examining protein conformational dynamics is the emerging technique of site-directed spin labeling (SDSL) (*32*−*34*). We sought to determine whether SDSL was sufficiently sensitive to detect ligand-induced conformational changes in the ER. In this technique, a uniquely reactive cysteine is inserted into, or remains in, a protein following substitution mutagenesis. This allows for the attachment of a spin probe at a specific site by using a thiol-reactive tether. The environment of the spin probe is then monitored using electron paramagnetic resonance (EPR). Motional freedom of the probe, its solvent accessibility to paramagnetic species, and distance-dependent interactions between spin-labels have all been used to interrogate the environment of the protein at the site of spin labeling (*35*, *36*), but spin probe mobility, in particular, has been used to evaluate the conformational character of non-membrane-associated proteins.

To explore the use of SDSL as a tool for evaluating ligand-induced conformational changes in the ER, we have attached nitroxide spin-labels to two specific sites in human ERα ligand-binding domain (hERα-LBD) mutants, allowing us to attach a label at either residue C530 or residue C417. We subsequently used EPR spectroscopy to monitor the environment of the spin-label in ER complexes with a variety of ER ligands. The spectra obtained demonstrate that ligand-induced changes in the ER are seen by SDSL/EPR spectroscopy, that these changes are complex, and that spectral analysis can be used to correlate these changes with the known pharmacological and structural characteristics of the ligands that were tested. Interestingly, raloxifene and *trans*-hydroxytamoxifen, two ER ligands of the SERM (selective estrogen receptor modulator) class that have different pharmacological activities yet produce similar ER crystal structures, exhibited different EPR spectroscopic characteristics. The results obtained here demonstrate that subtle conformational differences can be detected by SDSL, and that SDSL is able to produce meaningful results when applied to the ER. We believe this technique is a useful addition to current methods for evaluating ligand-induced conformational changes in the ER.

MATERIALS AND METHODS

Reagents, Plasmids, and Mutagenesis. The preparation of the wild-type human ERα ligand-binding domain (hERα-LBD) (amino acids 304−554) in a pET-15b vector has been described previously (*11*). All mutant ERs were derived from the same human ERα-LBD in a pET-15b vector. Mutant ERs were prepared such that either two or three of its reactive cysteines were mutated to serine. A fourth cysteine (C447), buried deep within the protein, is unreactive to labeling (*37*) and was unchanged. Mutant constructs C381S/C417S, C381S/C530S, and C381S/C417S/C530S were created as described elsewhere (*38*). The two ER double mutants are designated as *C530* and *C417* to highlight the site of the single reactive cysteine. Estrone (E_1) [3-hydroxyestra-1,3,5(10)-trien-17-one], estradiol (E_2) [estra-1,3,5(10)-triene-3,17*β*-diol], estriol (E_3) [estra-1,3,5(10)-triene-3,16α,17*β*-triol], 4-*trans*-hydroxytamoxifen (TOT) (1-{4-[2-(dimethylamino)ethoxy]phenyl}-1-(4-hydroxyphenyl)-2-phenylbut-1(*Z*)-ene), and α-zearalanol (P1496) [2,4-dihydroxy-6-(6α,10-dihydroxyundecyl)benzoic acid *μ*-lactone] were purchased from Sigma-Aldrich (St. Loius, MO). ICI164,384 {*N*-*n*-butyl-11-[3,17-dihydroxyestra-1,2,5(10)-trien-7α-yl] *N*-methylundecamide} was a gift from A. Wakeling and ICI Pharmaceuticals (Macclesfield, U.K.). ICI182,780 [7*β*[9]-(4,4,5,5,5-pentafluoropentyl)sulfinyl-[nonyl]estra-1,3,5(10)-triene-3,17*β*-diol] was purchased from Tocris Cookson Inc. (Ballwin, MO). Chloromethyl estradiol (CME_2, ORG 4333) [11*β*-chloromethylestra-1,3,5(10)-3,17*β*-diol] (*39*) was a gift from Organon (Oss, The Netherlands). Cyclofenil (cyc) {4-[4-(hydroxyphenyl)cyclohexylidenemethyl]-phenol}, raloxifene (ral) ([6-hydroxy-2-(4-hydroxyphenyl)-benzo[*b*]thien-3-yl]{4-[2-(1-piperidinyl)ethoxy]phenyl}-methanone, hydrochloride), ethyl-pyrazole-triol agonist (pyr-ag) [4-ethyl-1,3,5-tris(4-hydroxyphenyl)-1*H*-pyrazole] (*40*), and ethyl-pyrazole-triol antagonist (pyr-antag) {1,3-(4-hydroxyphenyl)-4-ethyl-5-[4-(2-*N*-piperidinylethoxy)phenyl]-1*H*-pyrazole} (*41*) were synthesized in our laboratory.

Spin-labels employed in these studies included the methanethiosulfonate label [MTSL, (1-oxyl-2,2,5,5-tetramethyl-Δ^3-pyrroline-3-methyl)methanethiosulfonate] purchased from Toronto Research Chemicals (Toronto, ON); a "shortened chain" (SC) label [3-(iodomethyl)-2,2,5,5-tetramethyl-2,5-dihydropyrrol-1-oxyl] synthesized, according to the method of ref *42*, from the bromo precursor supplied to us by I. Grigor'ev (Novosibirsk Institute of Organic Chemistry); and 4-(2-iodoacetamido)TEMPO [IT, 4-(2-iodoacetamido)-2,2,6,6-tetramethyl-1-piperidinyloxy] purchased from Sigma-Aldrich.

Transformation of Mutant Plasmids into Competent Escherichia coli and Expression of Mutant Protein hERα-LBD-(304−*554).* The plasmids were transformed into competent

BL21(DE3)pLysS *E. coli* (Novagen, Madison, WI), grown, induced, and harvested as previously reported by our laboratory for wild-type ERα (*43*).

Purification and Labeling of Mutant hERα-LBD(304−554). Purification of hERα-LBD(304−554) mutant proteins was analogous to that previously described for the wild-type protein (*11*, *43*). Modifications involved using nickel−nitrilotriacetic acid (Ni−NTA) resin (Qiagen, Valencia, CA) in a batchwise method, which allowed the protein to be labeled and unreacted free label to be removed easily. The total amount of ER bound to the resin was determined by comparing the difference in the amount of ER that was applied to the amount of ER collected in the flow-through. This was measured via ^{3}H estradiol binding and assayed using a standard hydroxyapatite (HAP) assay (*43*, *44*). Subsequently, a 7−15-fold excess of spin-label (see below), in T/G buffer [50 mM Tris and 10% glycerol (pH 8.0)], was added to the ER bound on the resin and the mixture allowed to incubate overnight at 4 °C. The following morning, the resin was pelleted, the supernatant removed, and the resin washed four times with T/G buffer. After the resin was washed, protein was eluted using an elution buffer [1 M imidazole, 500 mM NaCl, and 20 mM Tris-HCl (pH 7.9)], and the eluate was dialyzed twice against T/G buffer containing 30% sucrose. In some instances, the dialyzed receptor was subjected to further purification by size exclusion chromatography using Sepharose G-25-containing PD-10 columns (Amersham, Piscataway, NJ), as directed by the manufacturer.

Characterization of the Labeled Receptor and Ligands. The total protein concentration in receptor preparations was determined by the Bradford assay (*45*). Protein activity was determined from tritiated estradiol binding which was performed with 1 nM receptor in T/G buffer containing 0.3 mg/mL ovalbumin at 4 °C for 1 h. Determination of K_d values was done using an incubation time of 3 h with various concentrations of [^{3}H]estradiol in the absence or presence of 100-fold unlabeled competitor. K_d values were determined for the receptor in T/G buffer, and for the receptor in T/G buffer supplemented with 30% sucrose, 0.01 M β-mercaptoethanol, or both. Free estradiol was removed using HAP. Receptor affinity was determined using the method of Scatchard (*46*). Previous values for full-length wild-type ERα were taken from refs *43* and *47*. SDS−PAGE using the Laemmli system (*48*) was employed to ensure the purified labeled receptor was homogeneous and of the appropriate molecular weight. Molecular weights were further confirmed by MALDI-MS and ESI FT-ICR MS.

Relative binding affinities (RBAs) of the ligands were determined by competitive radiometric binding assays with wtERα-LBD using 10 nM [^{3}H]estradiol as the tracer, as previously described (*43*, *49*). Incubations were carried out for 18−24 h at 0 °C, and HAP was used to absorb the receptor−ligand complexes. The binding affinities are expressed relative to estradiol, which is set at 100%. These values can be reproduced in separate experiments with a coefficient of variation of less than 0.3.

Coactivator Recruitment Studies. Coactivator peptide recruitment studies were conducted using a maleimide tetramethylrhodamine (MTMR)-labeled coactivator peptide, MTMR-ILRKLLQE-COOH (University of Illinois Biotechnology Center, Champaign, IL). To conduct functional coactivator recruitment studies, mutant ERα-LBD was purified to homogeneity on Ni−NTA resin and labeled with IT as described above. However, instead of the receptor being eluted from the resin, the ER was retained on the Ni−NTA resin and used to "pull down" the MTMR-labeled coactivator peptide in the presence of various ligands for the ER. A 25 μL slurry of receptor-bound Ni−NTA resin was equilibrated in T/G buffer [50 mM Tris-HCl and 10% glycerol (pH 8.0)], placed in separate tubes, and mixed with 25 μL of T/G buffer containing either vehicle or 20 μM ligand. The Ni−NTA-bound receptor was then incubated for 1 h at 0 °C. Subsequently, a 50 μL sample of MTMR-labeled coactivator peptide in T/G buffer was added, and samples were allowed to incubate for 1 h at 0 °C. Final concentrations of the fluorescent coactivator peptide and ligands were 50 and 10 μM, respectively. Ni−NTA resin was washed three times with 500 μL of T/G buffer containing either vehicle or 10 μM ligand. The bound receptor was eluted by incubation with 100 μL of strip buffer [100 mM EDTA, 0.5 M NaCl, 20 mM Tris-HCl, and 10 mM β-mercaptoethanol (pH 7.9)] for 1 h at 0 °C. Twenty microliters of the eluted receptor was placed in separate wells of a black 96-well Molecular Devices HE microtiter plate (Molecular Devices, Sunnyvale, CA). The fluorescence of the MTMR-labeled coactivator peptide was monitored using a Perkin-Elmer Life Science Wallac Victor^2 V 1420 multilabel HTS counter with Wallac 1420 workstation software (Perkin-Elmer Life Sciences, Inc., Boston, MA), with a 544/15 nm excitation and 590/10 nm emission filter pair. Data were analyzed using Prism 3.00 (GraphPad Software, Inc., San Diego, CA).

Incubation of Spin-Labeled Receptor with Ligand. Receptor was incubated in the presence of a 10−100 fold excess of ligand for at least 1 h at 4 °C prior to acquisition of EPR spectra. The proportion of excess ligand that was used was kept constant for each series of experiments that was performed, and is listed as varying due to differences in the concentration of individual ER preparations. Excess ligand was not removed from the receptor, so bound and free ligand were at equilibrium throughout the experiment. Ligands were prepared as stock solutions in *N*,*N*-dimethylformamide (DMF). The final DMF concentration in the ER−ligand incubations was kept constant at 7% (v/v) for all data shown here. This concentration of DMF has a minimal effect on ligand binding to the receptor (*50*). In some instances, small traces of a DMF-derived radical were observed initially in collected spectra. Line shape analysis of the spectra was consistent with the splitting of one nitrogen nucleus (17.0 G) and six equivalent protons from two methyl groups (14.8 G). These additional signals may have resulted from redox chemistry between DMF and trace metals in solution. Their magnitudes decreased with time when the solution was allowed to equilibrate, presumably because of the consumption of a necessary oxidizing species such as oxygen. When present, these signals were removed by subtracting a background signal of 7% DMF in buffer prior to analysis.

Acquisition of EPR Spectra. Labeled receptor preparations were allowed to equilibrate to room temperature for at least 5 min following incubation before EPR spectra were recorded. Spectra were recorded at X-band (9.5 GHz) using a Varian E-122 spectrometer equipped with either an aqueous

flat cell or a loop-gap resonator. Variable-temperature studies were performed using a Varian E-257 VT apparatus and liquid nitrogen. Except where noted, samples were run with a microwave power of 0.2 mW, a modulation amplitude of 0.6 G at 100 kHz, and sweep durations of 30 s. Spectra for the MTSL-labeled receptor were acquired with a loop-gap resonator for a total of 45 scans. Spectra of the MTSL-labeled receptor were also obtained at W-band (95 GHz) to evaluate whether unbound label was present (*51*, *52*). Spectra of the receptor labeled with 4-(2-iodoacetamido)TEMPO at position *C530* or *C417* were collected at room temperature using a flat cell. The data shown here were acquired for a total of 120−400 scans. For each sample, signal averaging was conducted for at most 5 h at room temperature to ensure that the ER remained active and the instrument remained stable.

Variable-temperature studies of the free spin probes 4-(2-iodoacetamido)TEMPO (IT) and 3-(iodomethyl)-2,2,5,5-tetramethyl-2,5-dihydropyrrol-1-oxyl (SC) were performed to aid in determining optimal sweep widths for acquisition of spectra of the labeled receptor, and to evaluate parameters used in cross-correlational analysis (see below). Temperatures were measured with a thermocouple and ranged from −46 to 0 °C. These studies employed sweep widths of ≥160 G.

Analysis of EPR Spectra of Spin-Labeled ERs. The EPR spectrum of a nitroxide spin-label attached to ERs at X-band has a characteristic three-line pattern that results from hyperfine interaction between the ^{14}N nucleus and the unpaired electronic spin (*53*). However, it is the environment of a spin probe that produces a spectral line shape reflective of the motional character of the probe (*54*). In the fast motional regime, where the spin-label experiences rapid tumbling, a nitroxide will produce three equally spaced and equally intense narrow lines. As motion slows, the anisotropy of the hyperfine interaction becomes more apparent, and these peaks begin to broaden in a characteristic manner. At X-band, the high-field line ($m_I = -1$) is the first to broaden, followed by the low-field line ($m_I = +1$); the central line ($m_I = 0$) broadens but retains its original position and shape much more so than the other two. Eventually, as the label is placed into an environment that increasingly slows its motion (i.e., cooling), the spectrum will reach a rigid limit; at this point, the spectrum has the largest asymmetry and is spread out to its maximum extent. A useful method for characterizing motion from the fast through the slow regimes and to determine the rigid limit of a spin probe is to perform a variable-temperature study on the probe in question (*55*).

Addition of 30% sucrose to the spin-labeled ER preparations was necessary to slow protein rotational time. In the absence of sucrose, protein rotation contributed significantly to the spectra, resulting in spectra with a relatively intense, three-line spectrum having a narrow but m_I-dependent line width. This obscured changes in the broader spectral components by burying them in the baseline. Inclusion of 30% sucrose in the samples significantly reduced the magnitude of this sharp component. At this concentration, sucrose is not expected to affect the local motion of the spin-label relative to protein (*56*); rather, by slowing the global motion, and increasing the rotational correlation time of the protein, it allows the spectra to be more representative of the nitroxide side chain mobility relative to the receptor protein.

The dynamics of the nitroxide side chain are expected to depend on both the nitroxide side chain and the local protein structure at the nitroxide binding site (*57*). Rotational motion of the nitroxide can occur about any bond that links it to the protein. As such, the motion is expected to be both complex and highly dependent on the length and structure of the side chain (*58*) and is difficult to model or simulate using standard methods (*57*). The motion of the side chain is also expected to be anisotropic (i.e., the motion can be described as being ordered or restricted). Here, we use a qualitative model to analyze spectra, and as such, the term "motion" is used here in a general sense, to describe both the amplitude of motion and the restricted range of motion (*57*).

Standard Spectral Analysis for the Fast Motional Regime. In the fast motional regime, EPR spectra are often analyzed using an m_I-dependent line width formula

$$R_{2e}(m) = A + Bm + Cm^2$$

where R is the peak to peak line width of each of the three nitroxide peaks and $m = -1$, 0, or +1, corresponding to the line that is chosen ($m_I = -1$, $m_I = 0$, or $m_I = 1$). For a nitroxide, this analysis generates a series of three equations from which three unknowns (A, B, and C) can be solved. These values can then be either plotted by themselves or used with **g**- and **A**-tensor values (obtained from line shape simulation) and the experimental microwave frequency to solve for the nitroxide correlation time (*59*, *60*).

Adaptation of Fast Motional Analysis to the Intermediate-to-Slow Motional Regime. As one moves further through the intermediate-to-slow motional regime, it becomes difficult to measure the peak to peak line width of each line, because they broaden and become diffuse. As an alternative to measuring all three line widths, Todd and Milhauser (*61*) have expressed equations (to determine the B and C values of the m_I-dependent line width formula) in terms of the line width of the central peak, $\Delta B(0)$, and the peak heights of all three peaks, $V(+1)$, $V(0)$, and $V(-1)$. This allows one to measure B and C without needing to measure the peak-to-peak line width of the two outermost peaks. The two outermost peaks, $V(+1)$ and $V(-1)$, undergo significant broadening and are no longer well-defined in spectra of spin-labels exhibiting slow motion. This makes it difficult to measure their peak-to-peak line widths; however, their peak heights can still be measured very accurately. These expressions are as follows:

$$B = \frac{\sqrt{3}}{4}\Delta B(0)\left[\sqrt{\frac{V(0)}{V(+1)}} - \sqrt{\frac{V(0)}{V(-1)}}\right]$$

$$C = \frac{\sqrt{3}}{4}\Delta B(0)\left[\sqrt{\frac{V(0)}{V(+1)}} - \sqrt{\frac{V(0)}{V(-1)}} - 2\right] \quad (1)$$

Spectral Second Moment in the Analysis of the Intermediate-to-Slow Motional Regime. Recent literature of labeled proteins, with motion falling in the intermediate-to-slow motional regime, has made use of the measurement of the spectral second moment, eq 2 (calculated from the absorption spectra), and the peak-to-peak line width of the central line (*57*). The second moment is a good measure of inhomoge-

neous broadening, since its ΔB^2 dependency is very sensitive to diffuse lines.

$$\langle H \rangle^2 = \frac{\sum_i y_i \Delta B_i^2}{\sum_i y_i} \quad (2)$$

Relative Squared Difference Analysis. Two spectra can be compared relative to one another by calculating the relative squared difference (RSD) between them (*62*). RSD determinations performed in this study were from the algorithm shown in eq 3.

$$\mathrm{RSD} = \frac{\sum_i (a_i - b_i)^2}{\sum_i a_i^2} \quad (3)$$

This calculation is a sum of the spectral differences squared over a sum of the first spectra squared; *a* and *b* are the intensities of the two spectra being compared. The vertical scale of the *b* spectrum is adjusted to minimize the RSD. This algorithm can be applied to either the derivative or the absorption spectra (the first integral of the derivative spectra). Equivalent RSD values are produced if spectra are interchanged.

Statistical Analysis of Spectral Data. Statistical estimation of 95% confidence intervals for all data was carried out from the RMS *S*/*N* of acquired data and comparison to standard curves. Standard curves were constructed by determining the 95% CI versus RMS *S*/*N* for three separate *IT-417C* ligand−receptor pairs: unliganded *IT-417C*, E_2-bound *IT-417C*, and *IT-417C* bound by ICI182,780. Each preceding ligand−receptor pair was acquired in triplicate spectral runs of 10 × 50 scans for a total of 500 scans (collected as described above). Each 50-scan unit was sequentially summed to determine the RMS *S*/*N*. The *B* values, *C* values, and RSD between spectra were determined to construct the corresponding figures. In determining the 95% CI for RSD values, the following spectral pairs were compared: ICI182,780 versus ICI182,780, E_2 versus ICI182,780, apo versus ICI182,-780, E_2 versus E_2, E_2 versus apo, and apo versus apo. Thus, the RSD statistical analysis consisted of six sets by three runs by 10 scan values for a total of 180 comparisons. Correspondingly, the *B* value and *C* value analyses each consisted of three ligands by triplicate by 10 scan values for 90 individual values per analysis. The determination of the RMS *S*/*N* was checked for accuracy by plotting the square root of the scan number versus the experimentally determined RMS *S*/*N* (see Figures S1−S3 of the Supporting Information).

Software. Dataeg (*63*) was used to display, subtract, and compare spectra for normalization, to calculate line heights, line widths, second moments, and double integrals, and to perform relative squared difference (RSD) calculations (*62*). Ewvoigtn (*64*, *65*) was used to subtract sharp signals due to free label, particularly with spectra from the MTSL-labeled receptor. Receptor models were created with Sybyl (Tripos Inc., St. Louis, MO), by performing a simple MMF94s minimization on the spin-label attached to the protein while holding the protein as a fixed aggregate. Models are presented to give a sense of the likely environment of the spin probe and are not precise simulations.

RESULTS

Sites at Which the ERα-LBD Was Spin-Labeled Were Selected To Reveal Ligand-Induced Changes in ER Conformation

The ERα-LBD was labeled with iodoacetamidoTEMPO (IT) at position 417 or 530. The sites of labeling are illustrated with X-ray crystal structures of the dimeric ERα-LBD in either the agonist or antagonist conformation [from the E_2- and TOT-bound crystal structures] (Figure 1). From these models, it appears that the spin-label attached at C530 is in a much more mobile environment than the one at C417. There is also a large change in distance between the spin probes in the agonist and antagonist dimer structures when they are attached at C530 (13 vs 47 Å), whereas the interprobe distance at C417 changes very little between the two complexes. Of particular note is the fact that the C530 site is in a helical region in the agonist structure (the end of helix 11), whereas in the antagonist structure, it is in a loop region (between helix 11 and helix 12). These models are not precise simulations; they are static and unlikely to be exact representations of the spin-labeled ERs. Nevertheless, they do provide an overall illustration of where the sites of spin labeling are located within the ERα-LBD.

Ligands for This Study Were Selected To Represent Different Structural and Pharmacological Classes

We have selected a set of ligands, encompassing different core structures and pharmacologic classes and having different relative binding affinities, with which to examine how ligand binding to the ERα-LBD affects ER conformational dynamics. The structures of these ligands and their binding affinities for ERα are shown in Figure 2 and Table 1 (*66*).

Estradiol (E_2), estrone (E_1), estriol (E_3), and chloromethyl estradiol (CME_2) all have a similar tetracyclic steroidal core structure. Raloxifene (Ral) and 4-hydroxytamoxifen (TOT) are clinically important selective estrogen receptor modulators (SERMs), which show a differential agonism or antagonism depending on the tissue type. The X-ray structures of their complexes with the ERα-LBD are very similar, but the ligands have different core structures and significantly different pharmacological activities, with TOT (the active metabolite of tamoxifen) being more agonistic than raloxifene in a number of tissues (*67*, *68*). ICI164,384 and ICI182,780 are pure antagonists. The two ethyl-pyrazole-triol compounds (pyr-ag and pyr-antag) included here are novel heterocyclic ligands that have identical core structures. The pyr-ag is an agonist, but the pyr-antag with a basic side chain is an antagonist (*40*, *41*). P1496 (zearalanol) is an estrogen of unusual structure derived from the microbial metabolite zeralenone.

Preparation and Characterization of Site-Specific Spin-Labeled Mutant ERs

Preparation of Labeled Mutant ERs. The ligand-binding domain of ERα is a 31 kDa protein containing four cysteine residues, one of which (C447) is deeply buried within the

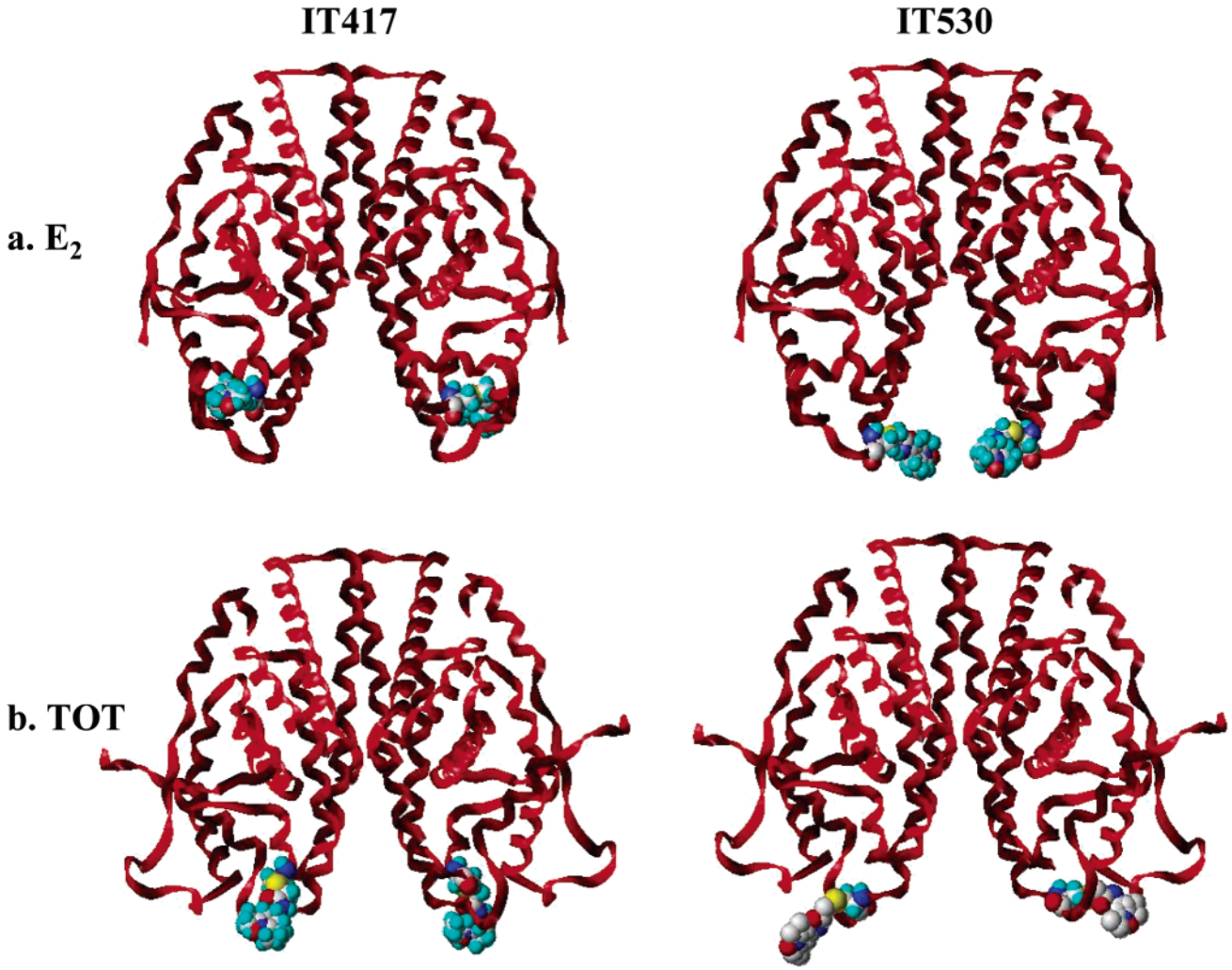

FIGURE 1: Models of spin-labeled estrogen receptor α. The hERα-LBD labeled with the iodoacetamidoTEMPO (IT) spin-label at positions 417 and 530 in (a) agonist (estradiol bound) and (b) mixed antagonist (4-hydroxytamoxifen bound) conformations. Models were created from known crystal structures (PDB entries 1ERE and 3ERT, respectively) by mutating residues 381 and 417 or 530 with serines, adding the spin-label, and performing a minimization on the spin-labeled residue while holding the protein constant.

protein and is unreactive toward thiol alkylating agents (*37*). In connection with a related project (*38*), we have prepared two ERα-LBD cysteine to serine double mutants. These are designated *C417* and *C530* to indicate the site of the single reactive cysteine remaining in each mutant, and it is to the remaining reactive cysteine residue (i.e., C417 or C530) that we have attached the following spin-labels: the methanethiosulfonate (MTSL), 3-(iodomethyl)-2,2,5,5-tetramethyl-2,5-dihydropyrrol-1-oxyl (SC), and 4-(2-iodoacetamido)TEMPO (IT) (Figure 3). (A triple cysteine to serine mutant, C381S/C417S/C530S, was also prepared as a control.) The mutant ERs were expressed in *E. coli* from a pET15b plasmid and were purified using a nickel resin via an N-terminal His_6 tag, as previously described (*43*). Conveniently, covalent labeling with the spin-labels can be done during purification, while the ERs are still immobilized on the nickel resin (*38*). This facilitates the removal of the unreacted spin-label, which would artificially narrow line widths in EPR spectra.

Physical Characterization of Labeled Mutant ERs. The labeled and purified ERs appeared as single bands on SDS−PAGE with an M_r of ca. 31 000 Da; there was little evidence of impurities from both Coomassie blue and silver staining. The molecular masses of the labeled ERs, determined by matrix-assisted laser desorption ionization time-of-flight mass spectrometry (MALDI-TOF MS), are summarized in Table 2. Masses were also confirmed by electrospray ionization Fourier transform ion cyclotron resonance mass spectrometry (ESI FT-ICR MS) and showed excellent agreement with their expected values, to within 0.00098% error (data not shown). All of the labeled proteins had masses fully consistent with that predicted for singly labeled species; labeling efficiency also appeared to be in excess of 95%, based on analysis by MALDI-TOF MS. To establish that there was no labeling at other sites in the ERα-LBDs, we exposed the triple cysteine to serine mutant C381S/C417S/C530S, which should have no reactive cysteines, to the same labeling protocol. After being labeled, the triple mutant produced only a very weak EPR signal at X-band, which was estimated to be <5% of that of the corresponding *C417* and *C530* spin-labeled ERs.

Functional Characterization of Labeled Mutant ERs. Protein and quantitative radioligand binding assays showed that the various labeled ER preparations could be prepared as pure proteins, at concentrations of ∼15−30 μM, retaining 65−91% of their theoretical maximum binding activity ([^{3}H]-E_2 binding per total protein concentration). We have attempted to obtain the highest activity levels in our receptor preparations, and most of them were well above the 65%

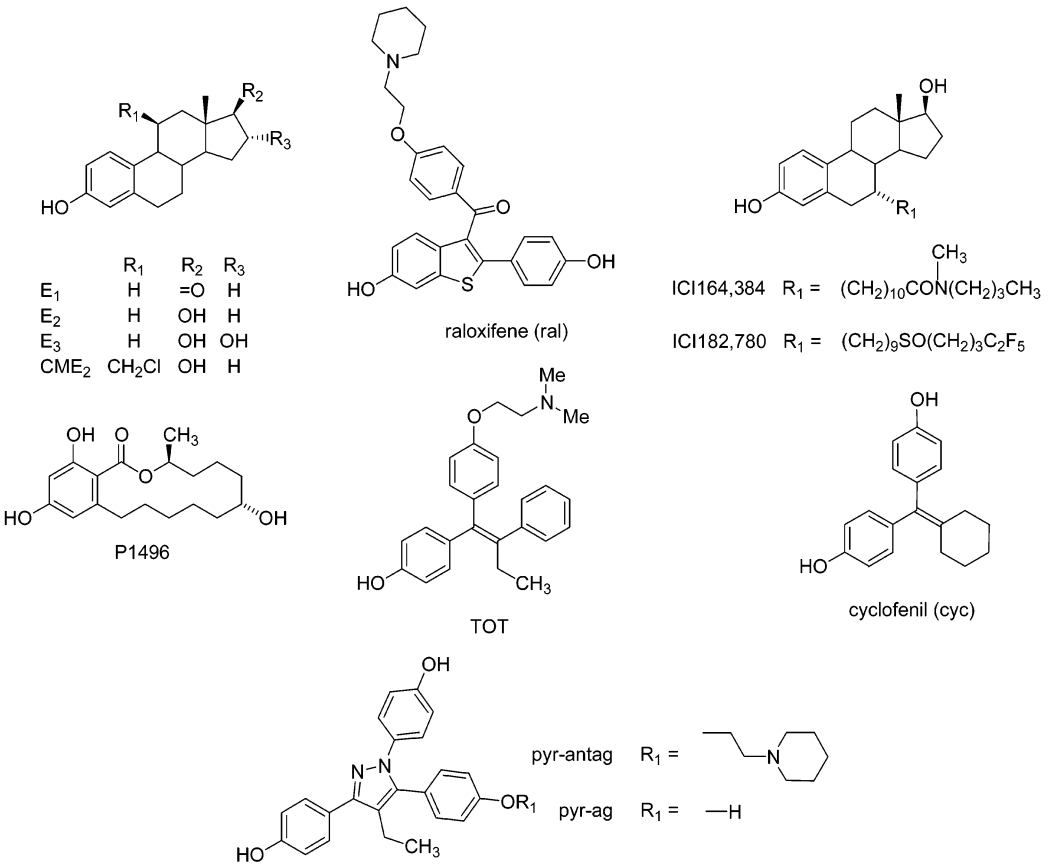

FIGURE 2: Structures of selected ligands. Chemical structures for estrone (E_1), estradiol (E_2), estriol (E_3), chloromethyl estradiol (CME_2), α-zearalanol (P1496), raloxifene (ral), 4-hydroxytamoxifen (TOT), ICI164,384, ICI182,780, cyclofenil (cyc), ethyl-pyrazole-triol agonist (pyr-ag), and ethyl-pyrazole-triol antagonist (pyr-antag).

Table 1: Relative Binding Affinity (RBA) Data for Ligands[a]

compound	RBA	compound	RBA
E_2	100	ICI182,780	75 ± 26 (5)
E_1	4.6 ± 0.5 (2)	cyclofenil	152 ± 8 (5)
E_3	7.1 ± 0.7 (2)	TOT	144 ± 18 (3)
CME_2	210 ± 10 (2)	raloxifene	41 ± 2 (2)
P1496	9.8 ± 2 (2)	pyr-ag	62 ± 2 (2)
ICI164,182	98 ± 20 (2)	pyr-antag	23 ± 3 (2)

[a] The number of assays is given in parentheses. All assays were performed at 0 °C for 18−24 h. Values were determined with a competitive radiometric binding assay with [^{3}H]estradiol and the ERα-LBD, as described in Materials and Methods.

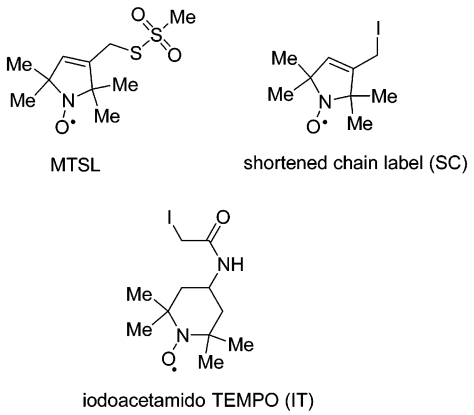

FIGURE 3: Structures of selected spin-labels. Chemical structures for MTSL, iodoacetamidoTEMPO (IT), and the shortened chain (SC) label used in this study.

lowest level we note. More significant, however, is that all of the experiments shown for both *IT-C417* and *IT-C530* have been performed upon single batches of the labeled receptor. Thus, any inactive receptor present was constant throughout the experiments and would add equally to all of the spectra obtained. Furthermore, since there is no way to model the EPR spectra an inactive receptor would produce, there is no way to subtract it. Separate experiments, using ethanol, urea, or guanidinium to denature the receptor, produce EPR spectra with very sharp lines, which are unlike what we observe for any of the data shown here.

The estradiol binding affinities of the IT spin-labeled ERs and unlabeled ERs were determined by Scatchard analysis and are summarized in Table 3. The affinities of the spin-labeled *IT-C417* or *IT-C530* were only somewhat lower than that of wild-type ER-LBD, and very similar, in T/G buffer, to those of the unlabeled mutant receptors. It is unclear why the triple mutant (C381S/C417S/C530S), when subjected to the same labeling and purification procedure as *IT-C417* and *IT-C530*, has an affinity closer to that of the wild type than either of the unlabeled mutants. The triple mutant was shown to be <5% labeled by EPR spectroscopy. The pattern of affinities measured in T/G buffer without sucrose was mirrored in buffer supplemented with 30% sucrose (data not shown). β-Mercaptoethanol is typically included in ER preparations to keep the protein in a reduced state. However, it cannot be used with spin-labeled proteins, because the nitroxide would be reduced by the thiol. Omission of β-mercaptoethanol, tested independent of addition of 30% sucrose, had little effect on the binding affinity or capacity of the wild-type or spin-labeled ERs (data not shown).

Table 2: Summary of Mass Spectral Analysis of Unlabeled and IodoacetamideTEMPO-Labeled ER-LBDs Used in This Study

receptor[a] preparation	observed[b] mass (Da)	expected[b] mass (Da)	mass accuracy (ppm)
C417	30 853.16	30 857.12	128
IT-C417	31 073.69	31 068.41	169
C530	30 852.62	30 857.12	162
IT-C530	31 069.78	31 068.41	44

[a] *C417* and *C530* represent ER double mutants C381S/C530S and C381S/C417S, respectively. *IT-C417* and *IT-C530* represent the *C417* and *C530* ERs labeled with IT, respectively. [b] Expected masses are for mono-labeled ERs; observed masses were taken from MALDI-TOF spectra.

Table 3: Summary of Estradiol Binding Affinity Data for Labeled and Unlabeled IodoacetamideTEMPO ER-LBDs Used in This Study

receptor preparation	K_d[d] (nM) in T/G buffer with ovalbumin and β-mercaptoethanol
ERα-LBD[a]	0.143
C417[b]	0.576
IT-C417[b]	0.575
C530[b]	0.297
IT-C530[b]	0.285
C381S/C417S/C530S[c]	0.131

[a] In previous publications (*43*, *47*), we and others have reported K_d values for full-length ERα of 0.36 ± 0.07 and 0.62 ± 0.09 nM, respectively. [b] *C417* and *C530* represent ER double mutants C381S/C530S and C381S/C417S, respectively. *IT-C417* and *IT-C530* represent *C417* and *C530* ERs labeled with IT, respectively. [c] C381S/C417S/C530S represents the triple ER mutant in which C381, C417, and C530 have all been changed to serine, which has been subjected to the same labeling procedure as *IT-C530* and *IT-C417*. [d] ERα-LBD was incubated at 0 °C for 3 h with various concentrations of ^{3}H-labeled estradiol in the absence or presence of a 100-fold excess of unlabeled estradiol. Aliquots of the incubation solution were measured to determine the total concentration of [^{3}H]estradiol present. The incubation solutions were then treated with hydroxylapatite and washed, and the concentration of bound [^{3}H]estradiol was determined. Values presented here have a CV of <0.15.

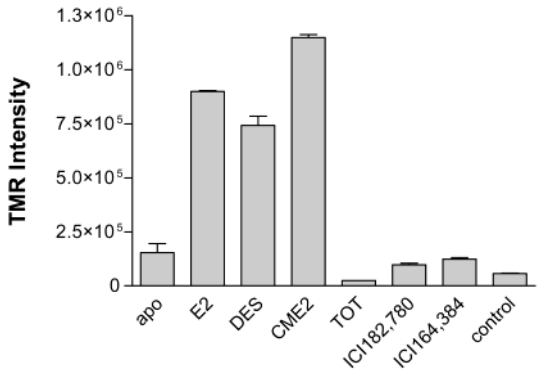

FIGURE 4: Coactivator peptide recruitment assay. A maleimide tetramethylrhodamine (MTMR)-labeled coactivator peptide was significantly recruited to agonist (E_2, DES, and CME_2)-bound iodoacetamidoTEMPO (IT)-labeled ER. There was little peptide recruitment seen with antagonist (TOT, ICI164,384, and ICI182,-780)-liganded IT-ERs. Apo indicates unbound ER, and control indicates no ER was added.

To determine whether labeled receptors retained wild-type functionality, we performed a ligand-dependent coactivator peptide recruitment study (Figure 4). This involved the ligand-dependent binding of a fluorescently labeled octapeptide. The octapeptide was derived from the sequences of GRIP-1 (glucocorticoid receptor interacting protein-1) and SRC-1 (steroid receptor coactivator-1) proteins. Analogous peptides have been shown by X-ray analysis to cocrystallize with the receptor when agonist ligand is bound, and to be recruited to the ER in a ligand-dependent fashion. The MTMR-labeled peptide was found to significantly bind to the receptor in the presence of the agonist ligands estradiol (E_2), chloromethyl estradiol (CME_2), and diethylstilbesterol (DES). Little to no binding was found while the receptor was unliganded (apo), bound by the pure antagonist ligands ICI182,780 and ICI164,384, or bound with the mixed antagonist *trans*-hydroxytamoxifen (TOT) (see Figure 4). Furthermore, we have previously reported that the analogous fluorescently (*Fl*) labeled receptors (*Fl-C417* and *Fl-C530*) are also able to directly recruit the coactivator peptide in a ligand-dependent fashion (*38*).

EPR Spectroscopy of Site-Specific Spin-Labeled Mutant ERs

Ligand Binding Induced Characteristic Changes in EPR Spectra of IT-C417 and IT-C530 ERs. A representative set of EPR spectra of IT-labeled ERs in 30% sucrose, bound with various ligands, is shown in Figure 5. The spectra have been normalized according to their central peak heights, and an enlargement of the low-field and high-field regions of selected *IT-C417* spectra is shown below. The term apo is used to refer to the receptor to which no ligand was added.

The relatively broad peaks in these spectra show that the IT spin-label attached to ERs undergoes significant slow motional broadening. Overall comparison of spectra for *IT-C417* spin-labeled ERs with those of *IT-C530* spin-labeled ERs shows that the IT label is exhibiting slower motion at position 417 than at position 530. This is evidenced by the diffuse and broadened low-field ($m_I = -1$) and high-field ($m_I = +1$) features of the *IT-C417* spectra, as compared to those of the corresponding spectra for *IT-C530*, which have lines with a narrower line width, making them appear to be sharper. Not only are the low- and high-field features broader in the *IT-C417* spectra, but they also can be seen to split apart, particularly the high-field feature. This splitting results from the anisotropy in the nitrogen hyperfine splitting and the *g*-factor. Splitting not only becomes more noticeable as the motion slows but also depends on the nature or dynamics of the motion itself. Spectra for spin-labeled ERs after incubation with ligand show nonidentical spectra for different ligands.

As one follows a series of ligands from agonists (E_2, P1496, and CME_2), through SERMs (TOT and Ral), to antagonists (ICI182 and Cyc), one notices changes in spectral broadening, with antiestrogens producing the broadest spectra (Figure 5). Spectra for agonist-bound *IT-417C* have distinct splitting of their low-field and high-field lines ($m_I = -1$, $m_I = +1$) that are unique, and thus distinct, from the other spectra (Figure 5, asterisk, low-field and high-field enlargements). This occurs because *IT-417C* spectra are in the intermediate-to-slow motional regime. Spectra in this regime are sensitive not just to the gross magnitude of motion they experience but also to the type, or order, of motion they experience. In comparison to the unique splitting seen with agonist spectra for *IT-417C*, broadening appears to be more similar for the series apo to SERM to antagonist for *IT-C417*, arguing that for these spectra, motion is more similar in type than for agonist spectra. An expansion of SERM (TOT and

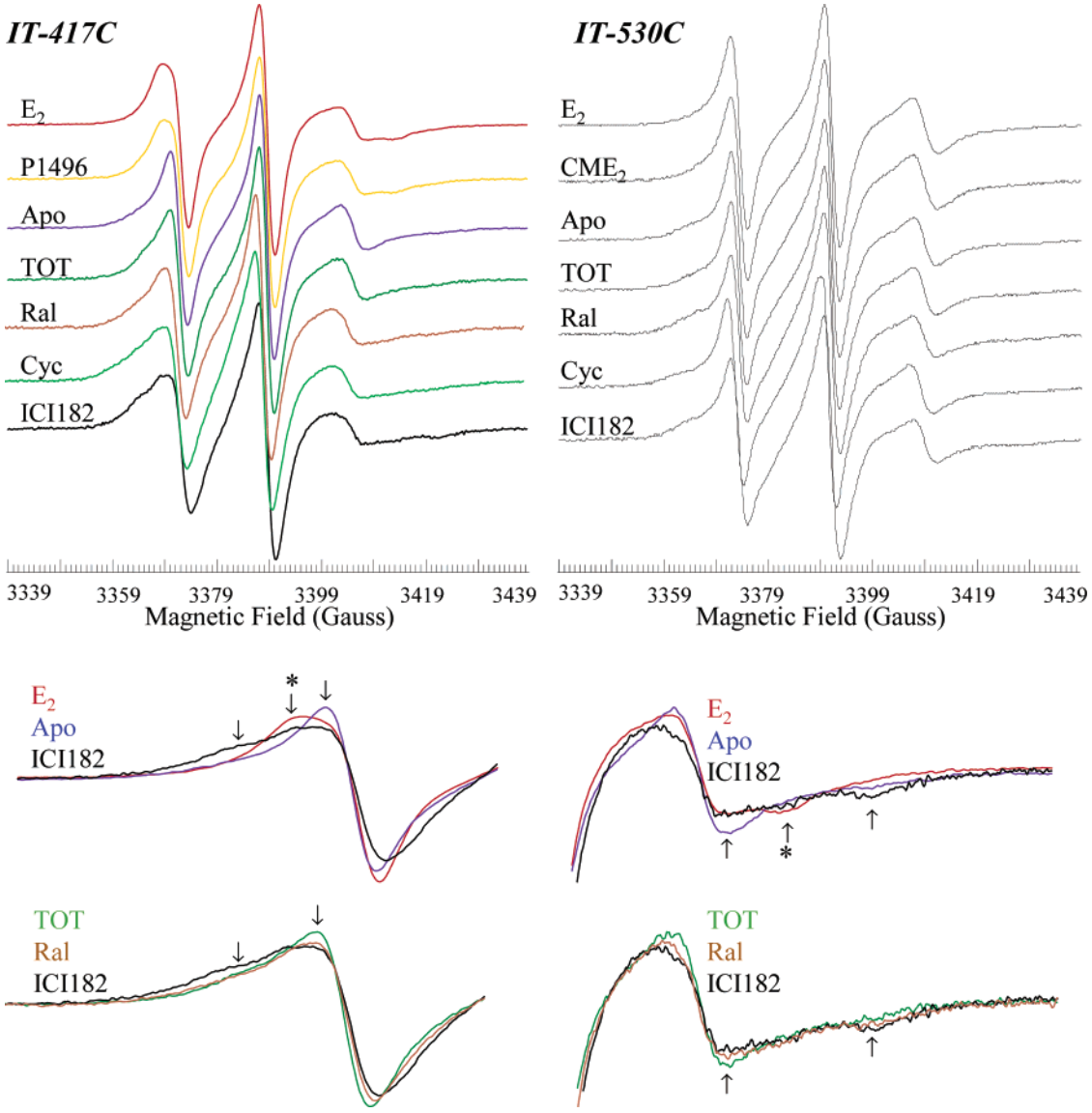

FIGURE 5: Representative spectra for *IT-C417* and *IT-C530*. Spectra that are shown are derivative spectra for unliganded and liganded *IT-C417* and *IT-C530*. The low-field ($m_I = -1$) and high-field ($m_I = 1$) lines have been expanded to show the slow motional broadening of selected *IT-C417* spectra. Arrows indicate predominate features due to slow motional broadening of the spin-label at position 417 (asterisks denote features unique to the agonist ligands). The microwave frequency was approximately 9.5 GHz. Each full spectra covers 100 G.

Ral) and ICI182,780 spectra illustrates this point for *IT-C417* (Figure 5). Therefore, motion undergone by the spin-label on agonist-liganded *IT-417C* appears to be of a type different from the motion seen for the series apo to SERM to antagonist.

From these spectra, it appears that the spin-label at position 530 is in the fast-to-intermediate motional regime, whereas the spin-label at position 417 is in the intermediate-to-slow motional regime. Spectra for *IT-417C* show an increased level of line broadening over spectra for *IT-530C*. (Note that the spectral parameters indicated by arrows in the high-field and low-field expansions for *IT-417C* are not as obvious on spectra for *IT-530C*.) Because the motion for *IT-C417* is much slower than for *IT-C530*, the spectra are not only dependent on the gross motion of the spin-label but also sensitive to both changes in the magnitude of motion and changes in the restriction of the range of motion. As a result, differences in motion between the various ligands can be ascribed to changes in line shape as well as overall line broadening changes, and the simple parametrization with *B* and *C* (see below) becomes less able to accurately distinguish changes in motion.

Cross-Correlation Plots of B versus C Allow One To Characterize the Conformational Mobility of Different Liganded ERs: Composite Plot of B versus C for IT-C417 and IT-C530 (Figure 6A). A composite plot of *B* versus *C* for *IT-C417* and *IT-C530* (Figure 6A) shows us a general comparison between labeling at position 530 and labeling at position 417. Points corresponding to *IT-C417* are found in the top right corner and demonstrate higher *B* and *C* values, whereas points corresponding to *IT-C530* are found at the bottom left with smaller *B* and *C* values. The higher the *B* or *C* value, the slower is the motion. Thus, we see that the spin-label attached to position 417 moves more slowly than the spin-label attached to position 530. Looking more closely at this graph, and the two graphs immediately below it (Figure 6B,C), one will notice a spread of data points corresponding to different ligand−receptor pairs, for both *IT-C530* and *IT-C417*. This shows that even when an identical position in ER is labeled, different ligands will

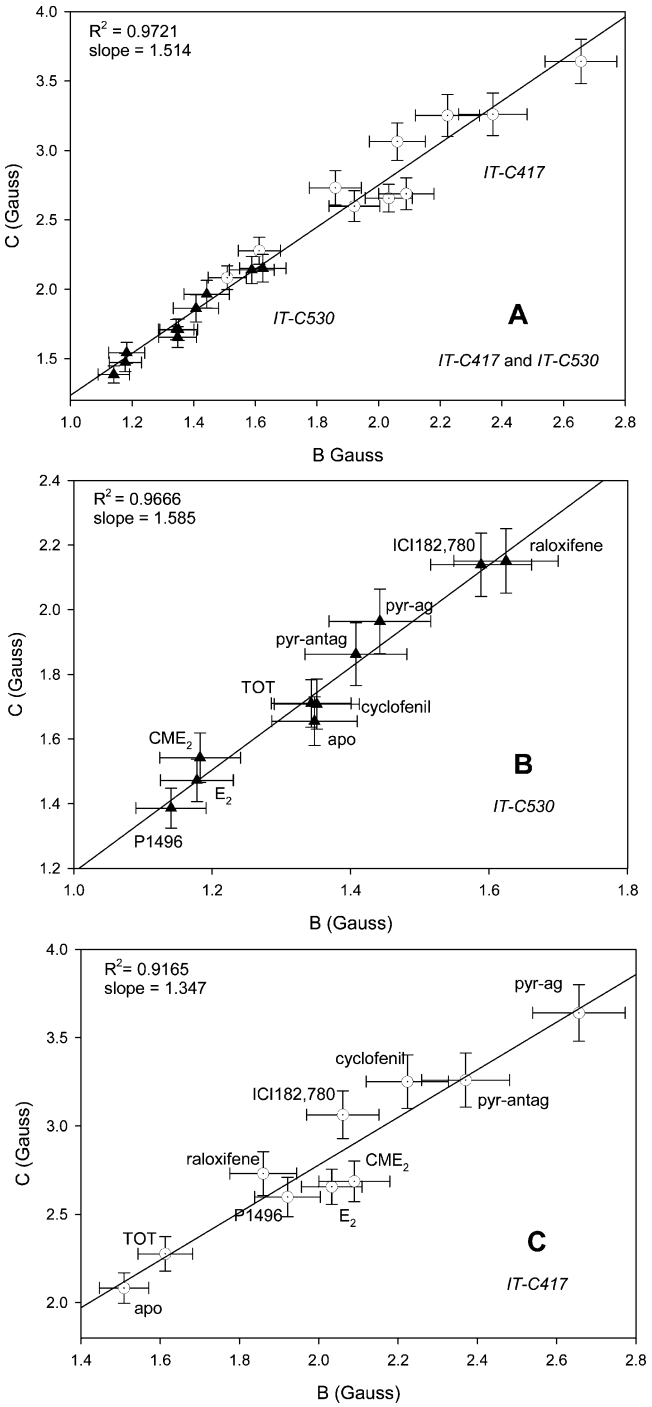

FIGURE 6: Slow motional analysis of the composite of *IT-C417* and *IT-C530* (A), *IT-C530* (B), and *IT-C417* (C). Slow motional analysis of the spin-labeled receptor was performed as per eq 1. Plots of *B* (gauss) vs *C* (gauss) produced linear correlations with R^2 values of 0.9721, 0.9666, and 0.9165. Spectra for *IT-C417* exhibited slower motion, producing higher *B* and *C* values. In contrast, *IT-C530* spectra showed faster motion. CIs (95%) are shown with cross-marks, and were determined as described in the text.

produce differences in the mobility of the spin-label. In addition to either accelerating or slowing the motion of the attached spin-label, a ligand bound to the receptor causes conformational changes which lead to the spin-label interacting uniquely with the protein (i.e., through steric, hydrophobic, and/or charge-based interactions).

Specific Plot of B versus C for IT-C530 (Figure 6B). Looking more closely at *IT-C530* (Figure 6B), we notice that ligands show groupings. In the bottom left corner, we find the three agonistic ligands: estradiol (E_2), chloromethylestradiol (CME_2), and P1496; E_2 and CME_2 share the same steroidal core structure, whereas P1496, a zearalenone derivative, has a core structure very different from that of a steroid (Figure 2). Though similar in structure, E_2 and CME_2 have very different affinities for the receptor, with CME_2 having a relative binding affinity (RBA) twice that of E_2 (see Table 1). Notable was the fact that none of the data from the EPR spectra, no matter which parameters were plotted, showed any correlation to RBA values. Therefore, the shape of the spectra was not simply influenced by ligand binding affinity.

As one progresses along the regression line, the next ligand−receptor pairs to be found are for the unliganded receptor (apo), *trans*-hydroxytamoxifen (TOT), and cyclofenil (cyc). Slightly further along are two compounds with a pyrazole core structure, abbreviated as pyrazole agonist (pyr-ag) and pyrazole antagonist (pyr-antag). *trans*-Hydroxytamoxifen (TOT) is a selective estrogen receptor modulator (SERM) that shows different degrees of partial antagonism depending upon tissue type; cyclofenil (cyc) also is a partial antagonist. Both have similar but also somewhat diverse structures consisting of a central alkene core off of which either phenol groups or modified phenol groups emerge in addition to alkyl substituents. The two pyrazole compounds are pharmacologically distinct from each other in their agonism or antagonism but here show a similar grouping, perhaps due to their identical core structure dominating the motion of the spin-label.

At the extreme top right-hand corner of the *B* versus *C* plot for *IT-C530* (Figure 6B), we find raloxifene and ICI182,780. The ICI182,780 compound is a full antagonist consisting of a steroidal core with a very large substituent at the 7α position. This substituent has been shown to displace helix 12 in the estrogen receptor (*69*). In fact, this displacement appears to be so complete that the helix remains unresolved in X-ray crystal structures of ERβ bound by ICI164,384 (*69*), a ligand with a structure very similar to that of ICI182,780 (Figure 2). Raloxifene, on the other hand, like TOT, is a SERM showing differing amounts of antagonism depending upon tissue type, but notably, raloxifene shows a higher degree of antagonism than TOT in several tissues (*67*, *68*). Raloxifene consists of a benzothiophene core with a basic side chain, which has also been shown to displace helix 12, thereby disrupting normal receptor function.

Interestingly, raloxifene and TOT do not produce equivalent EPR spectra for the receptor labeled at position 530; however, both of these ligands produce relatively equivalent crystal structures with only a few minor differences. From the point of view of dynamics and energetics, this might imply that raloxifene is much more efficient at disrupting the position of helix 12 than is TOT. This helps, in part, to explain the observed tissue differences seen between these compounds, as energy differences in the receptor would determine how stably the receptor interacts with coregulators. Overall, ordering of ligands on *B* versus *C* plots for the *IT-C530*-labeled receptor show a transition from agonism to SERM/partial antagonism to full antagonism, with the SERM raloxifene grouping near the pure antagonist ICI182,780.

Specific Plot of B versus C for IT-C417 (Figure 6C). Examining the plot of *B* versus *C* for *IT-C417* (Figure 6C),

beginning at the bottom left corner and following the regression line upward, one first sees TOT bound and apo (unliganded) receptor grouped closely together. Following the regression line further upward and to the right, we see in the center of the regression line that the three agonists, E_2, CME_2, and P1496, are tightly grouped. Also falling in the middle of the regression line are three ligand−receptor complexes in the order raloxifene, ICI182,780, and cyclofenil. Notice that each of these ligand−receptor complexes seems to have a distinct position on the plot. Moving further along the regression line, we find the two pyrazole-based compounds, the pyrazole antagonist (pyr-antag) and then the pyrazole agonist (pyr-ag).

As mentioned earlier, agonist-bound receptor structures for *IT-C417* exhibit a unique rounding of the low-field line that is not seen with the other receptor structures (see Ligand Binding Induced Characteristic Changes in EPR Spectra of *IT-C417* and *IT-C530* ERs). This phenomenon causes agonist spectra for *IT-417C* to have lower $V(-1)$ values and produce larger *B* and *C* values. Again, we stress the point that the line shape analysis formulas being used here are not rigorously valid outside of the fast motional regime, and the further one progresses into the slow motional regime, the less rigorous they become. Plotting *B* and *C* parameters is an approach to looking at the gross motion of a spin-label; it does not provide us with a picture of the type or order of motion undergone by a spin-label. As motion is slowed, the type or order of motion becomes more apparent in the EPR spectra. Visual inspection of agonist spectra shows they are similar to one another, and dissimilar from the spectra of other ligands that have been tested (Figure 5). A more effective analysis of the spectral differences at position 417, where significant slow motional broadening occurs, can be made by comparing spectra in their entirety, using a relative squared difference comparison (see below).

Relative Squared Difference (RSD) Analysis of Spectra Provides a Comprehensive Comparison between Spectra with Relation to Their Ligand−Receptor Identities. The equations used here to determine *B* and *C* values focus on changes in line height. Visual comparison of spectra of labeled ERs bound with different ligands shows that the shape of two spectra are different in many ways other than just line height, particularly for *IT-C417*-labeled ER spectra which show slower motion than *IT-C530*-labeled ER spectra (Figure 5). Often, spectra will be more different in one region (i.e., the low-field line, $m_I = -1$), and less different in a second spectral region (i.e., the high-field line, $m_I = 1$), because the broadening of these lines is related differently to the motional speed of the label (see Analysis of EPR Spectra of Spin-Labeled ERs in Materials and Methods). In layman's terms, the second spectral region is not as good as a "window" of motion as the first for observing differences between these spectra. In response to this issue, we sought a method that could complement the *B* and *C* value analysis presented above, that would be simple to apply, and that would be powerful enough to enable us to analyze the spectra in their entirety, yet still remain sensitive to spectral differences.

To satisfy these ends, we focused on the calculation of spectral second moments ($\langle H \rangle^2$) and the relative squared difference (RSD) between spectra. As mentioned earlier, we found that second moments were not able to produce the

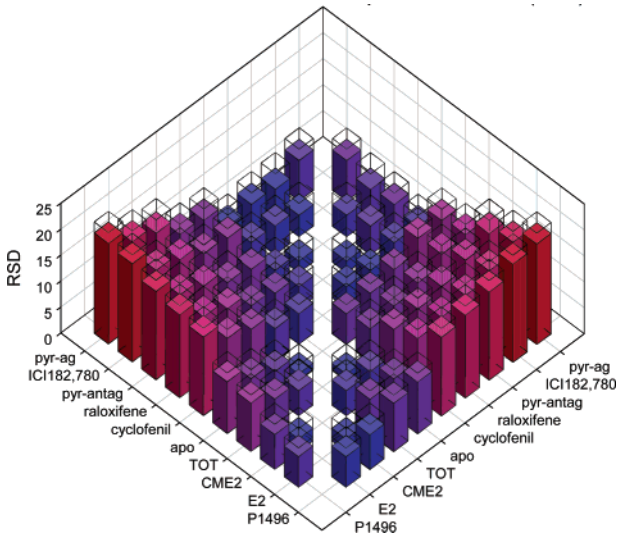

FIGURE 7: Relative squared difference (RSD) for *IT-C530* in 30% sucrose. A least squares plot of RSD based on a sum of variances calculation. The ordering of ligands was based upon ordering with respect to P1496. Clear boxes represent 95% CI values.

distinctions for which we had hoped when analyzing our spectra (data not shown). Thus, we focused instead on calculating the relative squared difference (RSD) between spectra (eq 3). This parameter compares total spectral differences between two different spectra. Similar to the calculation of a second moment, it views the spectra as a whole. Unlike second moment calculations, however, it is less sensitive to noise and baseline; because it has an $f(B)^2$ dependence rather than a ΔB^2 dependence, it is more resistant to noise, and the baselines of similar spectra tend to cancel out in this calculation.

The RSD, however, only provides a comparison between two spectra, and thus poses the question of how to select the proper reference spectrum as the basis for comparison. To avoid this issue, we have mapped the RSD between all possible pairs of EPR spectra for *IT-C417* and *IT-C530*. Constructing three-dimensional bar plots of these RSD values allowed us to conveniently evaluate differences and similarities between the spectra (Figures 7 and 8). Plotted this way, the higher the bar, the larger the difference is between a pair of spectra; correspondingly, the smaller the bar, the smaller the difference is between a pair of spectra. What one observes are valley-like plateaus representing similarity, and mountainous peaks representing difference.

RSD analysis of *IT-C530* (Figure 7) reveals several interesting characteristics. Generally, agonist versus antagonist comparisons produce large RSD values, suggesting large spectral differences, whereas antagonist versus antagonist or agonist versus agonist comparisons produce smaller values, suggesting spectral similarity. When specific points are examined, agonist-bound *IT-C530* ERs (E_2, CME_2, and P1496) form a plateau of similar spectra, with spectra for the P1496-bound receptor being slightly more different from the other two, perhaps due to its unique nonsteroidal core structure. The SERMs, TOT and raloxifene, produce spectra of moderate similarity, with spectra for the TOT-bound *IT-C530* ER being much more similar to those of the unliganded (apo) *IT-C530* receptor than those of raloxifene-bound *IT-C530*. On the other hand, raloxifene-bound *IT-C530* spectra are more similar to those of the pure antagonist ICI182,-

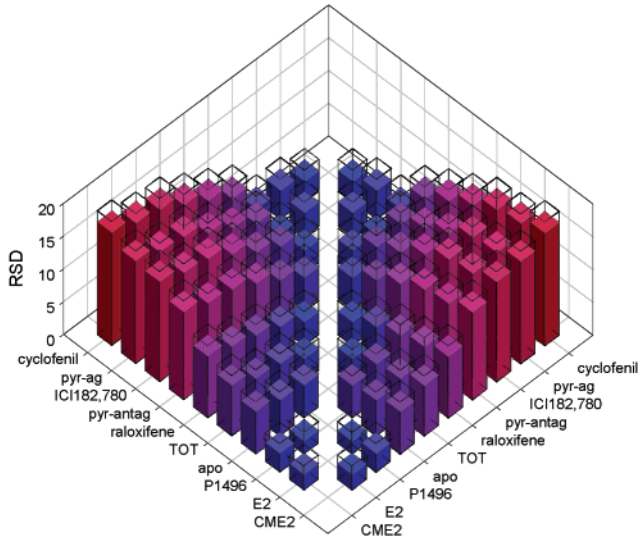

FIGURE 8: Relative squared difference (RSD) for *IT-C417* in 30% sucrose. A least squares plot of RSD based on a sum of variances calculation. The ordering of ligands was based upon ordering with respect to CME_2. Clear boxes represent 95% CI values.

780-bound receptors than to TOT or apo spectra. In addition to agonist-bound receptors producing a plateau of similarity for IT-C530, raloxifene, the two pyrazoles, and ICI182,780-bound receptors also produce a plateau of similarity. It is unclear why the receptors bound with the pyrazole compounds group so closely, and why both group nearer the antagonists than agonists; perhaps it is due to their pyrazole core structures. When cross-comparing agonist-bound receptors with antagonist-bound receptors, we find that CME_2 (along with E_2 and P1496) produces high RSD values when compared to raloxifene, cyclofenil, and ICI182,780, and vice versa. This indicates that the agonist *IT-C530* structures are very different from the antiestrogen structures.

The three-dimensional plot of the relative squared differences for *IT-C417* (Figure 8) produces a related ordering of compounds, but with certain differences. Again, the agonist (E_2, CME_2, and P1496)-bound receptors produce a plateau of similarity, but here we see less difference between P1496 and E_2-bound *IT-C417*, or CME_2-bound *IT-C417*, than was seen with the *IT-C530* ERs. Using RSD analysis (in contrast to the *B* versus *C* plots), we find that the differences between the three agonist ligands (E_2, CME_2, and P1496) and ligands with which they were grouped using *B* versus *C* analysis (raloxifene and ICI182,780, Figure 6C) are readily apparent in the larger RSD values for the respective ligand pair comparisons. This indicates that RSD analysis is preferable to the construction of *B* versus *C* plots for analysis of spectra in the intermediate-to-slow motional regime. The SERMs, TOT and raloxifene, appear to be similar as well, with TOT again being more similar to the apo receptor than is raloxifene, but the raloxifene-bound receptor being more similar to the full antagonist ICI182,780 than is TOT. With the *IT-C417* ER, however, raloxifene is still somewhat more similar to TOT than it is to ICI182,780, thus differing from its relation at position *IT-C530*.

These two figures (Figures 7 and 8) emphasize the fact that, while there are similarities in ligand ordering and grouping between *IT-C417* and *IT-C530* receptors, there are unique differences as well. For example, whereas TOT and raloxifene produce a relatively low RSD value for *IT-C417*, they produce a much larger RSD for *IT-C530*, indicating structural differences in the receptor at position 530 are greater than those at position 417 between these two ligands. Similarities should be expected, because the spin-label is probing the LBD bound to pharmacologically and/or structurally similar ligands. However, because the spin-label is probing different residues and areas of the LBD, there should be regional differences as well. These plots emphasize that calculation of the RSD can provide one with a quick overview of the degree of difference and/or similarity between two EPR spectra, especially when alternative methods of analysis are not sensitive for the intermediate-to-slow motional regime.

DISCUSSION

In this study, we have employed a relatively recently introduced novel method, substitution mutagenesis along with site-directed spin labeling (SDSL), for monitoring and evaluating protein conformational changes. This work shows the utility of EPR as a technique for the analysis of subtle, and biologically meaningful, ligand-induced conformational changes, for the estrogen receptor. Conformational changes were produced by binding ligands with diverse structures and pharmacology to the receptor, and they were measured at two distinct positions (*C417* and *C530*). Fortuitously, these two residues are cysteines in the native sequence, and they are also close to the ligand binding pocket; therefore, one would expect EPR signals from spin-labels tethered to these sites to reflect ligand-induced conformational changes. Independent evaluation of the spin-label at each position showed correlations between spectral differences and ligand structure and pharmacology. Both positions produced results that were both, in part, similar as well as distinctly different, highlighting the fact that the motional effects on the spin-label producing the spectra for each location and/or ligand are not the same. Thus, both sites are related yet distinctive, and each ligand is unique in its ability to change receptor conformation.

Obtaining Meaningful EPR Spectra from Spin-Labeled ERs

Selection of the Spin-Label and the Inclusion of Sucrose. In our initial studies with spin-labeled ERs, we used the disulfide-linked MTSL spin-label, which has been employed extensively by Hubbell and co-workers (*33*). The spectra of MTSL-labeled ERs, however, contained a three-line intense, sharp signal with a narrow line width that confounded our attempts to analyze ligand-induced spectral changes. We were unable to diminish the magnitude of this signal by further purification, suggesting that it was not free spin-label remaining in solution from our purification and labeling procedures. We believe that this signal was instead due to free MTSL released by disulfide exchange that could occur at the pH used for these studies (pH 8). To avoid this problem, we discontinued the studies with MTSL and concentrated on the behavior of ERs irreversibly labeled with 4-(2-iodoacetamido)TEMPO (IT). We obtained the largest spectral differences between different liganded receptors with IT-labeled ER and the inclusion of 30% sucrose. Sucrose was included in spin-labeled ER preparations to slow down protein rotational time (see Analysis of EPR Spectra of Spin-Labeled ERs in Materials and Methods).

Mechanism by Which the IT Spin-Label Measures Ligand-Induced Conformational Changes. To help us understand how the IT spin-label was functioning, we tested the role of the length of the tether linking the spin-label to the receptor. We labeled the receptor with a nitroxide spin-label that has a tether, shorter by two carbons than that for IT, linking it to the protein backbone; we have called it the "shortened chain" (SC) label (Figure 3). When *SC-C417* and *SC-C530* were evaluated, spectral differences (visual inspection and RSD calculations) were much smaller than with the IT label. Since rotational motion of the spin-label can occur about any bond that links it to the protein, the motion is expected to be both complex and highly dependent on the length and structure of the label that was used (see Analysis of EPR Spectra of Spin-Labeled ERs in Materials and Methods).

The SC label provides insight into the mechanism by which the IT label produces spectral differences. We believe that the shortened tether linking the spin-label to the protein does not allow SC sufficient interaction with surrounding residues to be highly sensitive to ligand-induced conformational changes; i.e., it is less effective in surveying changes in the microenvironment. It does, however, suggest there may be an optimal tethering linkage for observing meaningful changes in the EPR spectra. In this case, having a spin probe that is further from the peptide backbone of the protein allows the probe a larger axis about which to rotate, producing a larger cone of interaction with the side chains of neighboring residues (*32*). In our studies here, the shape and flexibility of the larger interaction cone with the IT spin-label (compared to the SC label) are better able to probe the protein surface in a manner such that ER conformational features correlate meaningfully with the pharmacology and structure of the bound ligands.

Choosing Spectral Parameters. Various spectral parameters were tested to evaluate the ligand-induced motional changes seen here. Recent studies on proteins in the slow motional regime have used the width of the central line ($m_I = 0$) and the spectral second moment ($\langle H \rangle^2$) as parameters for cross-correlation plots (*57*). However, though the central line width is a sensitive parameter of motion, its magnitude does not vary much; therefore, noise has a greater effect on it than on other measures. Noise was a factor in our experiments. Because of the limited solubility of the ER, spectra were recorded at concentrations (20−50 μM) that are relatively low for standard X-band EPR spectroscopy. Furthermore, determining the spectral second moments ($\langle H \rangle^2$) of the data here showed few meaningful trends, possibly due to slight baseline inconsistencies or noise. Because of its ΔB^2 dependence, the spectral second moment is sensitive to baseline variation and to noise because the parts of the spectrum furthest from the center add significantly to the calculation. Even though signal averaging produced reasonable spectra (average RMS $S/N = 456$) with apparently flat baselines (cf. Figure 5), either this level of noise and variation in baseline was too great, or the subtlety of motional differences was insufficient, for second moment calculations to provide us with consistent or meaningful results.

Additionally, since the spectra shown here have undergone significant broadening, it is difficult to apply the more traditional $R_{2e}(m) = A + Bm + Cm^2$ formula used when describing faster motion. This formula requires determining the peak-to-peak line width of each of the three lines. In the spectra shown here, it is unclear how to measure the line widths of the low-field and high-field peaks, because they are very broad and thus poorly defined. However, since there was considerable variation in the magnitude of peak heights in the spectra that are shown, we decided to use a method by which peak heights could be used as an alternative to measuring peak-to-peak line widths. Thus, we chose to use the two formulas for determining *B* and *C* values shown in eq 1, as derived by Todd and Milhauser (*61*) (see *Adaptation of Fast Motional Analysis to the Intermediate-to-Slow Motional Regime* in Materials and Methods). We emphasize that we are using the *B* and *C* values determined by these formulas as purely qualitative measures of motion. Since the speed of motion exhibited by spin-labeled ERs was in the fast-to-intermediate (for *IT-C530*) and the intermediate-to-slow regime (for *IT-C417*), the *B* and *C* values determined from these formulas cannot be used to estimate correlation times accurately (for a more detailed discussion see, Results). However, since the *B* and *C* values determined here were greater than 1.0 for all samples, it is reasonable to assume that the corresponding correlation times are all longer than a few nanoseconds (*70*).

Statistical Analysis of Spectra. Because of the large number of ligands surveyed and the time and sample required to obtain EPR spectra, statistical analysis was performed by analyzing the RMS *S*/*N* of each spectra and comparing this to a standard curve for the 95% CI for measured parameters (Figures S1 and S2 of the Supporting Information). Standard curves were created by evaluating the 95% CI (for *B* value, *C* value, and RSD determinations) for three ligand−receptor pairs (E_2, apo, and ICI182,780) as a function of the RMS *S*/*N*. To do this, each ligand−receptor pair was run, in triplicate, as a series of 10 sequential spectra consisting of 50 scans each. This resulted in three sets of 10 spectra (for each of the three ligand−receptor pairs above), with each set containing a spectrum representing 50, 100, ..., 450, and 500 scans. Thus, by performing triplicates and by sequentially summing each 50-scan spectrum, we could determine 95% CIs as a function of the RMS *S*/*N*. RMS *S*/*N* values were checked for consistency by plotting the aggregate RMS *S*/*N* versus the square root of the scan number for all statistical data collected (Figure S3 of the Supporting Information). The linear regression line ($R^2 = 0.996$) concurs that the RMS *S*/*N* was calculated correctly. We have normalized standard curves by the parameter they are plotting to ensure consistency for all data [i.e., (95% CI)/*B* value versus RMS *S*/*N*]. Statistical analysis of RSD values was essentially carried out as it was for *B* and *C* values; however, the spectra that were compared were those of ICI182,780 vs ICI182,780, E_2 vs ICI182,780, apo vs ICI182,780, E_2 vs E_2, E_2 vs apo, and apo vs apo. See Statistical Analysis of Spectral Data in Materials and Methods for further description.

Spectra of ER−Ligand Complexes in Relation to Ligand Structure and Pharmacology

The spectral groupings in the *B* versus *C* and the RSD plots correlate with both the pharmacology and structure of the ligands that were tested. *B* versus *C* and RSD plots present a general picture of agonist and antagonist ligands representing the extremes, with apo receptor and SERMs between them. The *B* versus *C* plots present this by linear organization of spectra, based upon their gross motion,

representing different liganded ERs (Figure 5). In contrast, the three-dimensional display of RSD values (Figures 7 and 8), based upon total spectral comparisons, produces plateaus and valleys of similarity and mountainous regions of difference among and between ligands of alike or different classes. The *B* versus *C* plot for *IT-C530* (Figure 6B) demonstrates this by placing agonist and antagonist ligands at the extremes of the plot. Interestingly, raloxifene groups closely with ICI182,780 in the *B* versus *C* analysis of *IT-C530* (see the discussion below). The *B* versus *C* plot for *IT-C417* presents a picture of apo to SERM to antagonist upon which the three tightly grouped agonist ligands (E_2, CME_2, and P1496) have been superimposed. As mentioned previously, spectra for agonist ligands at position *IT-C417* (Figure 5) show a unique splitting that is different from that seen with apo, SERMs, or antagonists; this characteristic splitting elevates their *B* and *C* values. We believe that this unique splitting in the agonist spectra from *IT-C417* results from the slower motion of the spin-label at this site than in *IT-C530*; this makes differences in the type, or order, of motion more apparent in the *IT-C417* spectra than in the *IT-C530* spectra, in which the probe exhibits faster motion. Again, *B* versus *C* analysis is typically applied to the fast motional regime and becomes less representative of spectra as motion is slowed. See Results for further description.

Estrogens E_1, E_2, and E_3 and CME_2 all have an identical steroidal core structure and are similar pharmacologically, though they have very different affinities for the receptor (5−210% of that of estradiol, Table 3). Data we have presented for E_2 and CME_2 show tight grouping with very little difference between spectra based on *B* versus *C* plots, RSD analysis, and visual inspection of overlaid spectra. In a similar series of experiments using the IT spin-label, the other physiologically relevant estrogens, estrone (E_1) and estriol (E_3), were also found to be very similar to E_2 and CME_2 (data not shown) (all data shown here were taken from a single batch of receptor; see Results). Curiously, P1496, a structurally unusual estrogen, grouped more tightly with the steroidal estrogens in the *B* versus *C* plots and the RSD calculations for *IT-C417* than for *IT-C530*. This suggests that with the P1496 ligand, the spin-label undergoes a motion at position 417 similar to that for steroidal agonists but that the motion of the spin-label at position 530 is slightly different.

Closer inspection of spectra for P1496 versus the steroidal estrogens at position 530 shows that the low-field and high-field lines are less broad, and that the valleys of the absorption spectra are also deeper for P1496 than for the steroidal estrogens. Overall, there is an equal line width narrowing over the entire spectral range for P1496 as compared to the steroidal agonists, which implies a similar type of motion, only faster. Because P1496 has an unusual structure compared to the steroidal estrogens (cf. Figure 4), it is not surprising that ER complexed with P1496 would undergo conformational dynamics that are different from those of the other ER−ligand complexes.

The SERMs raloxifene and TOT are well-separated in *B* versus *C* plots for both *IT-C530* and *IT-C417*. However, this separation does not appear to be quite as large in the *B* versus *C* plot for *IT-C417*. Interestingly, in the *B* versus *C* plot for *IT-C530*, raloxifene is grouped with ICI182,780, whereas in the *B* versus *C* plot for position *IT-C417*, raloxifene appears to be intermediate between the apo receptor and the ICI182,780-liganded receptor. In both *B* versus *C* plots, TOT appears to be close to the apo receptor. Comparing TOT and raloxifene using RSD analysis, we find that they produce a larger RSD (larger spectral difference) at position 530 than they do at position 417. On the basis of these observations, SDSL of the ER helps add insight into the mechanism of antagonism of raloxifene as compared to TOT. Compared to raloxifene, TOT lacks a second hydroxyl group and is thus unable to engage in hydrogen bonding with H524, a residue that is near the end of helix 11 and not far from C530. Thus, part of the greater motional freedom of the spin probe at position 530 in the TOT−ER complex versus the raloxifene−ER complex could result from elimination of this stabilization in the TOT complex.

For both TOT versus raloxifene and P1496 versus the steroidal estrogens, labeling at position 530 produced larger changes than labeling at position 417. This is consistent with the idea that this region of the receptor undergoes a more marked conformational change with ligands having varying degrees of agonist versus antagonist activity. Comparison of unliganded (apo), TOT, raloxifene, and ICI spectra (*B* versus *C* plots, RSD analysis, and visual inspection) shows that spectra for the TOT-bound receptor are closer to those of apo than are spectra for raloxifene or ICI (Figures 5−8) for both positions. In fact, of all the ligands that were surveyed, TOT is the closest to reproducing apo spectra, implying that at positions 417 and 530, the unbound receptor is very similar to the TOT-bound receptor. The spectral differences seen among apo, TOT, raloxifene, and the ICI ligands appear to be caused by faster motion of the spin-label. This trend followed an order [TOT (faster) > raloxifene > ICI (slower)] both with *IT-C417* and for *IT-C530*. As mentioned previously, this may imply that raloxifene, along with ICI182,780, is more efficient at disrupting the position of helix 12 from the point of view of energetics. This finding helps, in part, to explain the tissue-specific differences observed in the activity of these ligands (*67*, *68*).

The antiestrogen ICI182,780 produced very broad spectra. A similar series of experiments also using the IT spin-label, with both *C417* and *C530*, showed that ICI164,384 grouped closely with ICI182,780 (data not shown) (all data shown here were taken from a single batch of the receptor; see Results). In *B* versus *C* plots for *IT-C530*, raloxifene was grouped along with ICI182,780. RSD plots showed a plateau of similarity of ICI182,780 with the two pyrazole ligands, raloxifene, and cyclofenil for both positions that were studied. The two pyrazole ligands exhibited similar spectral characteristics, perhaps because their unusual, nonclassical heterocyclic core structure dominated the conformational changes being measured. This is feasible, because cyclofenil, an antiestrogen not containing a basic side chain, also falls in this region. The ICI compounds, which contain a side chain different from that of the SERMs, are believed to impede ER activity by a different mechanism, since helix 12 is unresolved in crystal structures of the ICI164,384-bound ER (*69*).

The results presented here support the generally accepted belief that ligands induce individual and unique conformations in the estrogen receptor and that estrogen receptor conformation is dynamic rather than static. They show that there is a correspondence between receptor conformation, as evaluated by the motional dynamics of EPR spin probes,

and the functional character of the ligands. Conformation is the structural key to receptor action and a major determinant of pharmacological character. It is not surprising, however, that there is not a perfect fit between ER conformation, as probed by SDSL/EPR spectroscopy, and ligand pharmacology, because the biological action of estrogens is multifaceted. It relies both on interactions that occur at various portions of the surface of the ER−ligand complex and on many downstream factors in the estrogen signal transduction cascade (*71*).

Site-Directed Spin Labeling as a New Method for Characterizing Nuclear Receptor Conformation

SDSL provides unique information that supplements the results obtained through other techniques by which conformational changes in nuclear receptors have been evaluated (coregulator interaction studies, protease sensitivity assays, fluorescence spectroscopy, X-ray crystallography, and NMR spectroscopy). All of these methods differ in their degree of resolution, and in being either dynamic or static. Deletion mapping of a protein sequence, along with coregulator interaction studies and phage display experiments, has been tremendously useful in helping to isolate the residues in a nuclear receptor which contribute the most to activity, and thus provide a starting point for investigating conformational change. Classical protease sensitivity assays provided some of the earliest insights into ligand-induced receptor conformational changes by demonstrating the apparent ease with which helix 12 can be trypsinized in the absence of ligand, and the greater rate at which helix 12 is cleaved in the presence of antagonists compared to agonists (ref *10* and our own unpublished work).

With the estrogen receptor, X-ray crystallography has illustrated the role of helix 12 as a primary determinant for agonist versus antagonist function. However, there are still many interesting ligands (including apo ER) for which no crystal structure exists, and pharmacologically different compounds (i.e., TOT and raloxifene) sometimes produce relatively similar crystal structures. Also, one should not forget that an X-ray structure is, in essence, a static snapshot of a single conformation out of what is likely to be a dynamic interchange of many conformations for an active protein breathing in solution.

Like X-ray crystallography, NMR spectroscopy has the potential to provide very high-resolution ligand−receptor structures, and it is a dynamic rather than static method. Still in its infancy with regard to nuclear receptor structure, NMR spectroscopy has generally shown that a ligand stabilizes the receptor (*25*), agreeing with protease sensitivity assays. In the future as it becomes easier to assign and determine distances between hydrogens, very highly detailed, dynamic pictures of receptor structure should become available using NMR methods.

Fluorescence and EPR spectroscopy are amenable to site-directed labeling, giving rise to the recent techniques of site-directed spin labeling (SDSL) and site-directed fluorescent labeling (SDFL). Some obvious advantages of fluorescent labeling over spin labeling include its high sensitivity and the ready availability of good instruments. The main disadvantage of fluorescence, when compared to EPR spectroscopy, is that routine fluorescence does not produce absorption (or derivative) spectra that contain as much spectral information as with EPR. In comparison to fluorescence data, EPR spectra allow for a greater analysis of line shape. Thus, fluorescence and EPR spectroscopy are supplementary to each other and are often used to evaluate similar phenomena, such as distances between labels (dipole−dipole interactions) and rotational correlation times (fluorescence anisotropy or EPR line shape analysis). Both of these techniques can provide moderate resolution of ligand−receptor conformational changes, with EPR spectroscopy potentially providing a higher resolution.

There are various constraints on SDSL that limit its practicality. Specialized and somewhat rare or exotic equipment is required. Experimentally, high protein concentrations are required to obtain a good signal-to-noise ratio, which may limit many experimenters. In our studies, we used a receptor concentration of 20−50 μM, which is at the lower end of the sensitivity scale for standard X-band spectroscopy. For many other protein systems, obtaining higher concentrations of the soluble protein might not be as difficult. We are hopeful, with increased availability and improved design of high Q-cavities, resonator cavities having very small energy losses at resonance, that this concentration requirement will diminish in the future.

In addition to the micromolar concentration requirement, SDSL requires that the interrogated protein be modified, so care must also be taken to ensure that wild-type functionality is retained with spin-labeled proteins. In the case of our studies on the estrogen receptor, this involved evaluation of its ligand binding activity and determination of the labeled ERs ability to recruit a coregulator peptide as a measure of downstream functionality. An advantage to such modification is that very few proteins (i.e., metalloproteins) have any intrinsic EPR absorption. Thus, background due to protein or buffer is relatively nonexistent, and one can be assured that any absorption seen is due to the spin-label on the site being modified.

From an EPR perspective, our work expands on the technique of SDSL by showing that SDSL can be used not only to evaluate different residues on a protein relative to one another but also to evaluate same-residue differences arising from ligand-induced changes. In effect, not only is it possible to distinguish between apples and oranges, but apples can be compared with one another as well. For the ER, not only can positions 530 and 417 be compared with one another, but SDSL can compare differences between individual ligand−receptor structures at each of these residues. In addition, this work shows that EPR spectroscopy can be used to study a soluble, active, and biologically complex protein (a receptor binding multiple ligands), helping to expand SDSL beyond the realm of the theoretician.

The interesting and novel information for various ER−ligand complexes that we have obtained using the technique of SDSL fits well with the current literature on nuclear receptor structure−function relationships. The results show that ligand-induced conformational changes in the receptor can be detected as changes in the mobility of the attached spin-labels. The exact mobility change that is induced is unique to the ligand that is bound, but in general, ligands of similar structure and pharmacological character induce similar mobility changes. This work also suggests that raloxifene may be better able to disrupt helix 12 than is TOT,

and that ICI182,780 is better than both of these at disrupting helix 12.

SDSL provides structural biologists with a unique addition to the currently available methods for determining protein conformational changes. As evidenced by the spectra obtained for TOT and raloxifene, this method can detect differences which may not be grossly apparent by visual inspection of a crystal structure. Since it involves a solution-based study of a probe placed directly on the receptor, it evaluates protein conformations in a direct manner that is sensitive to protein dynamics. The cross-correlation plots and relative squared difference plots presented here show a gradient of conformational change, supporting the view that receptor conformation is dynamic.

ACKNOWLEDGMENT

We thank the following people: Dr. Donald A. Seielsted, Dr. Ying R. Huang, Dr. Shaun R. Stauffer, and Christopher J. Coletta (for the synthesis of several of the ligands that were tested), Dr. Richard M. Milberg, Steve M. Patrie, and Dr. Neil L. Kelleher (for assistance with MALDI-TOF, and ESI FT-ICR MS analysis), and Dr. Alex I. Smirnov and Dr. Tatyana I. Smirnova (for valuable discussions and for assistance with acquisition of EPR spectra).

SUPPORTING INFORMATION AVAILABLE

Three figures pertaining to statistical analysis. This material is available free of charge via the Internet at http://pubs.acs.org.

REFERENCES

1. Nilsson, S., Makela, S., Treuter, E., Tujague, M., Thomsen, J., Andersson, G., Enmark, E., Pettersson, K., Warner, M., and Gustafsson, J.-A. (2001) *Phys. Rev. 81*, 1535−1565.
2. Weatherman, R. V., Fletterick, R. J., and Scanlan, T. S. (1999) *Annu. Rev. Biochem. 68*, 559−581.
3. Hall, J. M., Couse, J. F., and Korach, K. S. (2001) *J. Biol. Chem. 276*, 36869−36872.
4. Moggs, J. G., and Orphanides, G. (2001) *EMBO Rep. 2*, 775−781.
5. McDonnell, D. P., Clemm, D. L., Hermann, T., Goldman, M. E., and Pike, J. W. (1995) *Mol. Endocrinol. 9*, 659−669.
6. Trapp, T., and Holsboer, F. (1995) *Biochem. Biophys. Res. Commun. 215*, 286−291.
7. Kuil, C. W., Berrevoets, C. A., and Mulder, E. (1995) *J. Biol. Chem. 270*, 27569−27576.
8. Couette, B., Fagart, J., Jalaguier, S., Lombes, M., Souque, A., and Rafestin-Oblin, M.-E. (1996) *Biochem. J. 315*, 421−427.
9. Leid, M. (1994) *J. Biol. Chem. 269*, 14175−14181.
10. Leng, X., Tsai, S. Y., O'Malley, B. W., and Tsai, M.-J. (1993) *J. Steroid Biochem. Mol. Biol. 46*, 643−661.
11. Seielstad, D. A., Carlson, K. E., Katzenellenbogen, J. A., Kushner, P. J., and Greene, G. L. (1995) *Mol. Endocrinol. 9*, 647−658.
12. Elliston, J. F., and Katzenellenbogen, B. S. (1988) *J. Steroid Biochem. 29*, 559−569.
13. Katzenellenbogen, B. S., Elliston, J. F., Monsma, F. J., Jr., Springer, P. A., and Ziegler, Y. S. (1987) *Biochemistry 26*, 2364−2373.
14. Seielstad, D. A., Carlson, K. E., Kushner, P. J., Greene, G. L., and Katzenellenbogen, J. A. (1995) *Biochemistry 34*, 12605−12615.
15. Feng, W., Ribeiro, R. C. J., Wagner, R. L., Nguyen, H., Apriletti, J. W., Fletterick, R. J., Baxter, J. D., Kushner, P. J., and West, B. L. (1998) *Science 280*, 1747−1749.
16. Heery, D. M., Kalkhoven, E., Hoare, S., and Parker, M. G. (1997) *Nature 387*, 733−736.
17. Norris, J. D., Fan, D. J., Stallcup, M. R., and McDonnell, D. P. (1998) *J. Biol. Chem. 273*, 6679−6688.
18. Darimont, B. D., Wagner, R. L., Apriletti, J. W., Stallcup, M. R., Kushner, P. J., Baxter, J. D., Fletterick, R. J., and Yamamoto, K. R. (1998) *Genes Dev. 12*, 3343−3356.
19. McInerney, E. M., Rose, D. W., Flynn, S. E., Westin, S., Mullen, T. M., Krones, A., Inostroza, J., Torchia, J., Nolte, R. T., Assamunt, N., Milburn, M. V., Glass, C. K., and Rosenfeld, M. G. (1998) *Genes Dev. 12*, 3357−3368.
20. Hu, X., and Lazar, M. A. (1999) *Nature 402*, 93−96.
21. Paige, L. A., Christensen, D. J., Gron, H., Norris, J. D., Gottlin, E. B., Padilla, K. M., Chang, C. Y., Ballas, L. M., Hamilton, P. T., McDonnell, D. P., and Fowlkes, D. M. (1999) *Proc. Natl. Acad. Sci. U.S.A. 96*, 3999−4004.
22. Norris, J. D., Paige, L. A., Christensen, D. J., Chang, C. Y., Huacani, M. R., Fan, D., Hamilton, P. T., Fowlkes, D. M., and McDonnell, D. P. (1999) *Science 285*, 744−746.
23. Chang, C.-Y., Norris, J. D., Gron, H., Paige, L. A., Hamilton, P. T., Kenan, D. J., Fowlkes, D. M., and McDonnell, D. P. (1999) *Mol. Cell. Biol. 19*, 8226−8239.
24. Luck, L. A., Barse, J. L., Luck, A. M., and Peck, C. H. (2000) *Biochem. Biophys. Res. Commun. 270*, 988−991.
25. Johnson, B. A., Wilson, E. M., Li, Y., Moller, D. E., Smith, R. G., and Zhou, G. (2000) *J. Mol. Biol. 298*, 187−194.
26. Brzozowski, A. M., Pike, A. C., Dauter, Z., Hubbard, R. E., Bonn, T., Engström, O., Öhman, L., Greene, G. L., Gustafsson, J.-A., and Carlquist, M. (1997) *Nature 389*, 753−758.
27. Pike, A. C., Brzozowski, A. M., Hubbard, R. E., Bonn, T., Thorsell, A. G., Engstrom, O., Ljunggren, J., Gustafsson, J., and Carlquist, M. (1999) *EMBO J. 18*, 4608−4618.
28. Shiau, A. K., Barstad, D., Loria, P. M., Cheng, L., Kushner, P. J., Agard, D. A., and Greene, G. L. (1998) *Cell 95*, 927−937.
29. Egner, U., Heinrich, N., Ruff, M., Gangloff, M., Mueller-Fahrnow, A., and Wurtz, J. M. (2001) *Med. Res. Rev. 21*, 523−539.
30. Pike, A. C., Brzozowski, A. M., and Hubbard, R. E. (2000) *J. Steroid Biochem. Mol. Biol. 74*, 261−268.
31. Shiau, A. K., Barstad, D., Radek, J. T., Meyers, M. J., Nettles, K. W., Katzenellenbogen, B. S., Katzenellenbogen, J. A., Agard, D. A., and Greene, G. L. (2002) *Nat. Struct. Biol. 9*, 359−364.
32. Borbat, P. P., Costa-Filho, A. J., Earle, K. A., Moscicki, J. K., and Freed, J. H. (2001) *Science 291*, 266−269.
33. Hubbell, W. L., McHaourab, H. S., Altenbach, C., and Lietzow, M. A. (1996) *Structure 4*, 779−783.
34. Hubbell, W. L., Gross, A., Langen, R., and Lietzow, M. A. (1998) *Curr. Opin. Struct. Biol. 8*, 649−656.
35. Hubbell, W. L., Cafiso, D. S., and Altenbach, C. (2000) *Nat. Struct. Biol. 7*, 735−739.
36. Hustedt, E. J., Smirnov, A. I., Laub, C. F., Cobb, C. E., and Beth, A. H. (1997) *Biophys. J. 74*, 1861−1877.
37. Hegy, G. B., Shackleton, C. H., Carlquist, M., Bonn, T., Engstrom, O., Sjoholm, P., and Witowska, H. E. (1996) *Steroids 61*, 367−373.
38. Tamrazi, A., Carlson, K. E., Daniels, J. R., Hurth, K. M., and Katzenellenbogen, J. A. (2002) *Mol. Endocrinol. 16*, 2706−2719.
39. Bindal, R. D., Carlson, K. E., Reiner, G. C., and Katzenellenbogen, J. A. (1987) *J. Steroid Biochem. 28*, 261−370.
40. Stauffer, S. R., Coletta, C. J., Tedesco, R., Sun, J., Katzenellenbogen, B. S., and Katzenellenbogen, J. A. (2000) *J. Med. Chem. 43*, 4934−4947.
41. Stauffer, S. R., Huang, Y. R., Aron, Z. D., Coletta, C. J., Sun, J., Katzenellenbogen, B. S., and Katzenellenbogen, J. A. (2001) *Biol. Med. Chem. 9*, 151−161.
42. Hankovsky, H. O., Hideg, K., and Lex, L. (1980) *Synthesis*, 914−916.
43. Carlson, K. E., Choi, I., Gee, A., Katzenellenbogen, B. S., and Katzenellenbogen, J. A. (1997) *Biochemistry 36*, 14897−14905.
44. Williams, D., and Gorski, J. (1974) *Biochemistry 13*, 5537−5542.
45. Bradford, M. M. (1976) *Anal. Biochem. 7*, 248−254.
46. Scatchard, G. (1949) *Ann. N.Y. Acad. Sci. 51*, 660−672.
47. Wooge, C. H., Nilsson, G. M., Heierson, A., McDonnell, D. P., and Katzenellenbogen, B. S. (1992) *Mol. Endocrinol. 6*, 861−869.
48. Laemmli, U. K. (1970) *Nature 227*, 680−685.
49. Katzenellenbogen, J. A., Johnson, H. J. J., and Myers, H. N. (1973) *Biochemistry 12*, 4085−4092.
50. Katzenellenbogen, J. A., Heiman, D. F., Carlson, K. E., and Lloyd, J. E. (1982) in *Receptor-Binding Radiotracers* (Eckelman, W. C., Ed.) pp 93−126, CRC Press, Boca Raton, FL.
51. Nilges, M. J., Smirnov, A. I., Clarkson, R. B., and Belford, R. L. (1999) *Appl. Magn. Reson. 16*, 167−183.

52. Smirnov, A. I., Belford, R. L., and Clarkson, R. B. (1998) in *Biological Magnetic Resonance, Volume 14: Spin Labeling: The Next Milennium* (Berliner, L. J., Ed.) Plenum Press, New York.
53. Weil, J. A., Bolton, J. R., and Wertz, J. E. (1994) *Electron Paramagnetic Resonance Elementary Theory and Practical Applications*, Wiley & Sons, New York.
54. Petrakis, L. (1967) *J. Chem. Educ. 44*, 432−436.
55. Yruela, I., Alfonso, M., Garcia-Rubio, I., Martinez, J. I., Picorel, R., and Alonso, P. J. (2001) *Biochim. Biophys. Acta 1515*, 55−63.
56. Timofeev, V. P., and Tsetlin, V. I. (1983) *Biophys. Struct. Mech. 10*, 93−108.
57. McHaourab, H. S., Lietzow, M. A., Hideg, K., and Hubbell, W. L. (1996) *Biochemistry 35*, 7692−7704.
58. McHaourab, H. S., Kalai, T., Hideg, K., and Hubbell, W. L. (1999) *Biochemistry 38*, 2947−2955.
59. Freed, J. H. (1976) in *Spin Labeling Theory and Applications* (Berliner, L. J., Ed.) pp 592, Academic Press, New York.
60. Hwang, J. S., Mason, R. P., Hwang, L. P., and Freed, J. H. (1975) *J. Phys. Chem. 79*, 489−511.
61. Todd, A. P., and Milhauser, G. L. (1991) *Biochemistry 30*, 5515−5523.
62. Mueller, F., Grande, H. J., Harding, L. J., Dunham, W. R., Visser, A. J. W. G., Reinders, J. H., Hemmerich, P., and Ehrenberg, A. (1981) *Eur. J. Biochem. 116*, 17−25.
63. Nilges, M. (2002) *Dataeg*, version 3.03.
64. Smirnova, T. I., Smirnov, A. I., Clarkson, R. B., and Belford, R. L. (1995) *J. Phys. Chem. 99*, 9008−9016.
65. Smirnov, A. I., Smirnova, T. I., and Morse, P. D., II (1995) *Biophys. J. 68*, 2350−2360.
66. Gao, H., Katzenellenbogen, J. A., Garg, R., and Hansch, C. (1999) *Chem. Rev. 99*, 723−744.
67. Katzenellenbogen, B. S., and Katzenellenbogen, J. A. (2002) *Science 295*, 2380−2381.
68. Shang, Y., and Brown, M. (2002) *Science 295*, 2465−2468.
69. Pike, A. C., Brzozowski, A. M., Walton, J., Hubbard, R. E., Thorsell, A. G., Li, Y., Gustafsson, J., and Carlquist, M. (2001) *Structure 9*, 145−153.
70. Goldman, S. A., Bruno, G. V., and Freed, J. H. (1973) *J. Chem. Phys. 59*, 3071−3091.
71. Katzenellenbogen, J. A., O'Malley, B. W., and Katzenellenbogen, B. S. (1996) *Mol. Endocrinol. 10*, 119−131.

BI035566P